Biochemical-Physical Mechanisms of Light-Tissue Interactions

August, 2021

Biochemical-Physical Mechanisms of Light-Tissue Interactions

By

Musawenkosi Doctor Buthelezi, with student number of 209505646

A thesis submitted to the

University of KwaZulu-Natal

in fulfilment of the requirements for the degree

of

MASTER OF SCIENCE in PHYSICS

Supervisor: Prof Naven Chetty

Co-supervisor: Dr O Adeleye

UNIVERSITY OF KWAZULU-NATAL

SCHOOL OF CHEMISTRY AND PHYSICS

PIETERMARITZBURG CAMPUS, SOUTH AFRICA

Declaration – Plagiarism

I, Musawenkosi Doctor Buthelezi, declare that

1. The research reported in this thesis, except where otherwise indicated, and is my original research.

2. This thesis has not been submitted for any degree or examination at any other university.

3. This thesis does not contain other persons' data, pictures, graphs or other information, unless specifically acknowledged as being sourced from other persons.

4. This thesis does not contain other persons' writing, unless specifically acknowledged as being sourced from other researchers. Where other written sources have been quoted, then

(a) their words have been re-written but the general information attributed to them has been referenced, or

(b) where their exact words have been used, then their writing has been placed in italics and referenced.

5. This thesis does not contain text, graphics or tables copied and pasted from the internet, unless specifically acknowledged, and the source being detailed in the thesis and in the reference sections.

Student: [redacted] Date: 25 – Aug - 2021

Disclaimer

This work was undertaken as a Masters degree programme in physics at the University of KwaZulu-Natal, Pietermaritzburg campus. I take sole responsibility for the views and opinions expressed therein.

Student: Musawenkosi Doctor Buthelezi

Signature: 

Date: 29 November 2021

Supervisor: Professor Naven Chetty

Signature: 

Date: 30 November 2021

Co - supervisor: Dr Oluwabamise Adeleye

Signature: 

Date: 30-Nov-2021

Abstract

Optical tissue phantom samples simulating the optical properties of the human prostates and brain tissues were fabricated. The experimental set-up was designed to be cost-effective but reliable, allowing for convenience in its usage and replication, making it ideal for biomedical optical measurements. Gel agar was the base material, and aluminum oxide (Al_2O_3) with black ink was employed as the scatter and absorber, respectively. The latter were mixed in various amounts into the gel agar to simulate the desired phantom tissues. Argon red laser and He-Ne green laser light, with wavelengths of 630 nm and 532 nm were incident on varying thicknesses of the phantom samples. The transmitted and incident light powers were measured to determine the scattering and absorption coefficients, from which the attenuation coefficients, penetration depth, and optical albedo were estimated. The optical penetration depths were found to be 0.30 for brain and 0.15 for prostate tissue phantoms. The fabricated tissues successfully mimicked the brain and prostate tissues, with μ_a = 0.69 $\mathrm{cm}^{-1}$and μ_a = 0.24 cm^{-1} absorption coefficients as well as $\mu_s = 1.73\ \mathrm{cm}^{-1}$ and μ_s = 5.48 cm^{-1} scattering coefficients at 532 nm and 630 nm wavelengths, respectively. The optical albedo for brain phantom was found to be a = 0.71 and a = 0.96 for prostate phantom tissue. The results verify the reliability of the experimental technique and suitability of the fabricated tissues for use in biomedical, going forward, thus allowing for future work without the need for experimentally complex and expensive setups.

Acknowledgements

I wish to express my sincere gratitude to my Supervisor, Prof Naven Chetty for his patience, support and impeccable guidance throughout the duration of the project. He has been pushing me and making sure that I have done the work accordingly.

I sincerely thank my co-Supervisor, Dr Bamise Adeleye, a UKZN academic in the School of Chemistry and Physics from Pietermaritzburg campus, for the encouragement and guidance in my carrying out of this project work.

Lastly, I would like to thank my family and friends for the continuous support and encouragement.

Musawenkosi Buthelezi

Contents

List of Figures

List of Tables

Chapter 1

1.0 Introduction

1.1 Background Information

Biomedical imaging refers to numerous processes executed to give an anatomical cross-sectional and functional image of the human body for therapeutic and diagnostic purposes [1]. The need for clear images, free of distortion and blurriness, is vital for both the biomedical and medical sciences [2]. In recent years, significant developments in optics, lasers, and computational power have enabled the development of more accurate tissue phantom models, improving the fundamental scattering models previously in use. This has allowed for better investigations into the radiation interaction with organic materials such as skin, resulting in more realistic pictures [2].

Significant progress in fiber optics, lasers, and other related technologies has increased the popularity of subdermal imaging [2]. In biomedical sciences, relevant instrumentation, such as conventional X-ray, optical coherence tomography, near-infrared fluorescence, computerized tomography and magnetic resonance imaging, are required to analyze biological systems [3, 4]. The dominant factor is that the instrument's insertion must be non-invasive [5]. By viewing wavelengths of electromagnetic radiation passing through dermal tissue, it is possible to produce a picture of the human skin's subdermal layers for proper diagnosis [5].

Optical imaging techniques like coherence gated imaging, with conventional radiography film and ultra sonography, are also currently utilized to acquire high-resolution pictures of biological structures and their fundamental structure [6, 7]. For optical imaging, a property of radiation called scattering is exploited by measuring the intensity of light moving through a dermal tissue into the subdermal layers of the desired tissue [5]. Scattered light provides important chemical and biological information about the studied sample [5]. Dispersing light

through biological specimens is a feasible tool for diagnosing certain conditions, but this requires a visible electromagnetic wave scattering model in a specific complex medium [5].

The imaging of tissue simulating phantoms for near-infrared or optical spectroscopy started in the early 1980s with the rise of clinical curiosity in near-infrared transillumination for breast cancer imaging [8]. Furthermore, the interest also rose from application in photodynamic therapy, therapeutics planning, and pulsed laser therapeutics planning, where the optical fluence distribution information in tissue was crucial to attaining treatment efficiency [8].

In 1993, the introduction of time-resolved, frequency-domain light signals and spatially resolved light urged most scientists to investigate imaging and spectroscopy of a tissue, which led to numerous different tissue phantom types [8, 9]. In recent years, the uses of light in medical sciences have surged considerably with surgery. A cosmetic laser is now being used more frequently in procedures at both state and private facilities [8]. Reflectance and fluorescence diagnostics have also emerged as forerunners in the diagnostic realm [10]. Further research into luminescence imaging, near-infrared tomography, photodynamic therapy dosimetry, optical coherence tomography, and fluorescence molecular imaging, amongst other applications, is key to advancing the medical diagnosis and therapeutics [11]. Therefore, it is imperative that there is sufficient and significant progression in the development of suitable phantoms to further enhance the research.

Optical imaging is a diagnostic of molecular method including the usage of either optical coherence tomography or a near-infrared fluorescence to investigate phantom tissues from the tiny structures within the cell to the level of the organ, to verify bimolecular distributions inside the cells, for in vivo enzymes imaging and selective treatment of tumours and pathways [12]. Optical imaging fundamentally uses ultraviolet, infrared, and visible light sub-cellular and cellular molecular events for in vivo mapping [12]. These processes and techniques have notably lessened the exposure of the patients to harmful radiations by employing light emitting sources for systems assessments of the body [14]. Optical imaging is an essential technique because it is safer than ionizing radiation such as X-rays. They may be employed for repetitive events such as observing the progression of sickness or the treatment outcome.

Optical imaging is broadly performed in human tissue experimental trials, for example, skin, lung reconstruction, bladder, and brain [13]. These tissues are needed to be modeled or simulated with tissue phantoms to comprehend their optical properties. This is significant for the description of beams for a particular application or the choice of laser type and light propagation [14, 15]. A tissue-mimicking phantom is made of a base material with the addition of an absorbing agent and a scattering agent [16]. Georges et al. [17], 1997, intended to create optical phantoms with similar scattering and absorption coefficients as organic tissue under a comprehensive spectral range (410-650 nm) to optimize and model cancer photo-detection ways using light-induced fluorescence (LIF) spectroscopy. The phantoms, made with agar as base material, displayed fundamental parallels with the human tissues' optical characteristics, which is vital in the experimental context, where numerous wavelengths showing enormous propagation differences in organic tissues are included [11]. In 2006, Theodore et al., [18] to mimic the optical properties of organic tissues at wavelengths of 830 nm and 690 nm (visible and near-infrared spectral range), developed photostable and castable solid optical tissue phantoms containing absorbing chromospheres and polyurethane as a scattering agent. They found the difference in scattering and absorption properties for the experimental phantoms (twelve samples) to be about ±3% by optical properties consistent in 14 months, making them appropriate for usage as a reference standard.

1.2 Deflection or Diffusion of Particles

Scattering employing particles can be determined by classical electromagnetic theory [18]. Usually, the matter has no electric charge. Nevertheless, it is still composed of multiple discrete charges [18, 19]. Since light is an oscillating electromagnetic field, it can excite the charges in matter and cause them to vibrate. These oscillating charges then radiate electromagnetic waves, which are scattered waves. The superposition of the scattered waves with incident waves is observed. Coherent scattering occurs if the frequency of secondary waves is at the same or nearly similar source frequency [18]. Incoherent scattering occurs with unequal frequency of secondary waves.

It has been recognized that specular reflection takes place at plane surfaces, though the plane surfaces are uneven on the photon's scale [18]. The view of the refraction and incidence angles turns out to be challenging to clarify in this circumstance. Spread or specular reflection occurs when electromagnetic radiation reflects from an uneven surface with great irregularities; in this event, the reflected angles are approximately equal to the incident angles. Interpretation of scattering clarifies the refracted and reflected as the superposition of scattered secondary waves produced by incident wave [18]. The optical parameters themselves give essential information to guide tissue metabolic status or disease diagnosis, especially cancer [19]. Recently, many methods to measuring the optical tissue parameters have been developed. Most use radiation in the near-infrared and visible wavelength range. Biological tissues are mostly light scattering, typically highly forward-directed in the visible spectral range. In contrast, absorption is increased in the mid-infrared range of the spectrum because of the vigorous absorption characteristics of water molecules [19]. Currently, experimental procedures to investigate tissues are primarily based on measurements of the diffuse transmittance or reflectance: oblique-incidence optical fiber reflectometry, video reflectometry, and integrating sphere measurement [19].

1.3 Lasers and Light in Biological Systems

1.3.1 Background

When a laser beam is incident onto tissue, generally between 4 – 7% of the incident light is reflected directly. The others 93 – 96% of the light propagates into the organic tissue, where it may be absorbed, scattered, or transmitted [20, 21]. The degree to which heat is generated depends on the degree of photon absorption within the tissue [22]. For Nd: YAG (yttrium aluminum garnet) lasers (1060 nm) with moderately great wavelengths, 30 – 50% of the incident visible light re-emerges from the organic tissue [22]. YAG is a crystal situated within the laser employed for the technique. The technique is completed and simple on an outpatient basis in just a few minutes. As soon as the absorptive capacity is larger compared to its scattering capability, the laser stays firmly calibrated in the tissue, and the depth of the penetration turns into a wavelength function reliant on the absorption coefficient. Through

wavelengths identical to those of the argon laser (~500 nm), the scattering and absorption can be matching in cardiovascular tissue. Scattering usually is dominant in the red and infrared wavelength ranges. Blue light propagates wavelengths with lesser penetration depth than near-infrared and red wavelengths [22].

The primary exposure concerns to optical sources include unpleasant reactions like photoaging and numerous skin cancer types, chloriorental injuries, immune suppression, and photomutations [23]. A main photochemical effect of optical, electromagnetic wave exposure upon the eye and skin is skin reddening (such as the burning of skin) or erythema and keratoconjunctivitis (welder's flash) [24]. Electromagnetic radiation destroys tissue mainly by two mechanisms: thermally, by chemical bond variations due to high temperatures produced from electromagnetic radiation exposure and photochemically through variations in chemical bonds due to heat produced from radiation exposure [23]. Notably, the harm from photochemical interactions is important at high frequencies with transmission capability of a higher energy into tissue [25].

1.3.2 Low-Level Light Therapy (LLLT)

Photobiomodulation or Low-Level Light Therapy (LLLT) has been utilized for numerous medical procedures like swelling, traumatic brain injury, ophthalmology applications, and dentistry [26]. LLLT is also known as "soft or cold light" because the light that is propagated does not heat and ablate the tissue [26], use LEDs or specific lasers with intensity (or power density) changing from 780 – 1100 nm (near-infrared) and 400 – 700nm (visible light) wavelengths, and 5 – 500 nM/cm2 [26, 27]. The LLLT mechanism is based on the absorption of definite visible near-infrared and red wavelengths by biological photoreceptors situated within the human cells [26]. This irradiation type may be a low-dose pulsed light [26, 27]. The 700 – 780nm wavelength has been found ineffective as it matches the oxidase absorption spectrum. Furthermore near-infrared lights red (630 – 670nm) are mainly effective because of their broad penetration depth, absorption and lower scattering by chromospheres of the tissue [26].

1.3.2.1 Dentistry

Low-Level Light Therapy is used to help heal a wound, for the process of dentine repairing and stimulates the biological activity of human periodontal ligament stem cells proliferation and mesenchymal stem cells [28]. Chromium: Yttrium, Scandium Gallium Garnet, Erbium (Erbium Cromo lasers) in the infrared region has the capability of interacting with hydroxyapatite and water has been utilized in dentistry to handle both hard and soft tissues [29]. These lasers function in pulse mode, 140s pulse duration, and transport fiber with a diameter of 600m and 300 m pulse energy [29].

1.3.2.2 Ophthalmology

Laser is used in ophthalmology for various diseases, including posterior segments (seleral, retina) or anterior segments (iris, cornea, lens) of the eye. The important laser characteristics utilized in ophthalmology are the probability of varying the intensity, wavelength, spot size in the enormous range, and pulse duration. Thus, the laser-interaction may be optimized and changed to therapy (from diagnostics) in the very same tissue [30]. The advantage of another significant laser in ophthalmology is that it may be applied without any contact, making its functioning non-invasive [30].

1.3.2.3 Dermatology

In 1963, Leon Goldman pioneered the efficiency of lasers in treating different dermatological sicknesses [31]. His work led to the usage of numerous types of laser for different applications, ranging from surgical to aesthetic purposes and vascular malformations transformation, like removal of the tattoo, resurfacing of patients, and benign pigmented lesions removal [31]. The laser treatment advantages over usual treatment in dermatology like skin grafting and brain injuries are that the treated area remains sterile, giving an ideal bed for instant skin grafting. Additionally, blood loss is very minimal.

1.4 Importance of the Research

The exposure effect to ultraviolet radiation of definite biological tissues is a comparatively unexplored area. It is necessary that researchers start to document the damage caused. Laser light interaction with numerous biological tissues at specific wavelength requires further exploration and this work has been designed to address this matter. The main goal of this study was to create and develop phantom tissues with properties mimicking those of the human tissues. Phantoms usage is an efficient alternative in early tests of procedure and imaging devices since its variables dependency is introduced by real subjects [32]. The subsequent goal was to understand the penetration of laser light and interaction along with optical properties functions like refraction index, anisotropic factor, absorption, and scattering. These properties determine laser-tissue interaction mechanism in that particular case, enabling the new biomedical development therapeutic and diagnostic techniques.

1.5 Properties and Characteristics of Organic Tissues

Tissue, in biomedical terms, is described as a collection or group of cells with similar structure, operating within an organism. A collection of these tissues executing identical functions forms an organ. Therefore, tissue is the intermediate between cells and a complete organ. The principal organ of the human body is the skin, and it is often the focus of examination in biomedical science. The skin is inhomogeneous and multi-layered, thus making it hard to simulate [33]. A multi-layer skin model is developed to mimic wrinkling. This model consists of the underlying hypodermis, stratum corneum, and dermis. The model's findings can be compared with the outcome of the *in vivo* wrinkling tests experiment carried out on the volar forearm.

The deepest layer of the skin is known as the stratum corneum, and it ranges between 0.01 and 0.02 mm broad [33]. Stratum corneum cannot absorb a lot of light in the visible area of the electromagnetic spectrum, and incident light is largely transmitted. The epidermis is a

structure and is the second layer of the skin. It comprises of four layers, with total thickness ranging between 0.027 and 0.15 mm [33]. Generally, the epidermis absorbs or transmits light. The absorption is because of chromophore discovered in the epidermis, namely melanin. This chromophore is important because it is the chemical group that absorbs electromagnetic radiation at a particular frequency and, thus, imparts colour to a molecule. Melanin consists of two types: pheomelanin (yellow or red) and eumelanin (black or brown). Together, they absorb a range of frequencies, with greater absorption at higher frequencies. The eumelanin is responsible for the unique skin colour and the proportion between the pheomelanin concentrations, and varies between individuals. Melanin is produced by melanocytes situated within thin membranes known as the melanosomes. The radiation concentration absorbed by melanin relies on the volume of melanosomes in the epidermis [33].

The dermis is the third layer of skin, and it is roughly 0.6-3 mm thick. Similar to the epidermis, it also mainly transmits and absorbs light. This skin layer comprises blood vessels and nerves and is a dense connective and irregular tissue [5]. The blood cells comprise a chromophore: hemoglobin. This chromophore gives blood its red colour and absorbs light. The other two chromophores in the dermis comprise of bilirubin and beta carotene, which offer the skin a yellow or brownish color [5].

The final layer is the hypodermis, and it is usually not regarded as part of the skin. It has discrete sizes all over the body. This hypodermis has low absorption in the visible region and up to 3 cm thick in the abdomen. This layer comprises several fats. White cells reflect the incident light to the upper layers [33].

1.6 Purpose and Hypothesis of this Work

The challenges involved in investigating the optical properties of tissue *in vivo* are clearly defined. These challenges are mostly stochastic errors initiating from fluid blood, pulsation, temperature, sweatiness, and hydration effect measurements. Hence, *ex vivo* measurements

remain a better procedure for isolating tissue types. However, it is essential to consider the tissue hydration, blood drainage, and sample freshness [22]. An initial step in biophotonics development for tissue therapeutics and diagnostics is to comprehend the relationship between biological and optical properties of tissue [22].

Direct measurements are at times unattainable due to boundaries of accessibility and storage of fresh samples. Moreover, the results' reproductiveness may be inconsistent and, consequently, demanding the task of finding identical specimens [22]. Therefore there is another way of utilizing tissue-equivalent materials or phantoms. The optical attributes of the tissues may be simulated in a medium with the appropriate absorption and scattering coefficients. Typically, phantoms are layered structures or homogeneous and, thus, do not usually possess the complex structures of the tissues [22]. This work is very significant in other parts of medicine, such as cancer treatment with low laser pulses [22]. The experiment arrangement was designed to be as cost-effective as possible, while maintaining accuracy. A laser of wavelength 630 nm (red) and wavelength 532 nm (green) were incidents on phantom tissue samples of varying thickness [22]. Then, measurements to determine the transmitted and incident powers of the electromagnetic radiation were performed. Thereafter, the significant optical characteristics of the phantom tissues were determined.

SPECIFIC OBJECTIVES

- To examine the biochemical mechanisms of light-tissue interactions using inexpensive tissue phantoms.
- To define methods for characterizing laser beam propagation and laser dosimetry in tissue.

The creation of optical phantom samples formed the core of this work to mimic human tissues' optical properties.

A better understanding of the association of optical properties with the relevant organic tissue may allow methods to be developed in the curative and diagnostic uses of biomedical sciences [22].

Chapter 2

2.0 Theory

2.1 Significant Properties of Light

Reflection, absorption, transmission, and scattering are essential properties of light when considering light propagation through organic systems. Transmission is the electromagnetic radiation passing through an object [14]. Some materials do not transmit the entire incident radiation but absorb some radiation, typically converting it to heat. This property is absorption. The thicker the object, the more radiation is absorbed, and less radiation is transmitted with increased material thickness.

Reflection occurs when the light bounces off the incident surface and moves back into the source medium [14]. The laser light reflection is due to disparities in the refraction indices between tissue and air [13]. Scattering is when the light is incident on a rough surface and tends to transmit or reflect in many directions [14].

2.1.1 Reflectance, Transmittance, and Absorptance

The transmittance (T) of any medium is the ratio of the light's transmitted intensity (I_T) to the incident light intensity (I_0).

$$T = \frac{I_T}{I_o}. \qquad (2.1)$$

The ratio of the absorbed intensity I_A to the incident intensity is called the absorptance A of a medium.

$$A = \frac{I_A}{I_o}. \qquad (2.2)$$

The ratio of the reflected intensity I_R to the incident intensity is the reflectance of a medium R:

$$R = \frac{I_R}{I_o}. \quad (2.3)$$

For a medium that absorbs only a small fragment of incident radiation and simultaneously transmitting the rest or vice versa, this holds;

$$I_o = I_T + I_A + I_R, \quad (2.4)$$

Here I_R, I_T, I_A depends on wavelength [10]. Therefore

$$R(\lambda) + T(\lambda) + A(\lambda) = 1 \quad (2.5)$$

2.1.1.1 Transmittance Measurement

Light transmission through gases, fluids, and optical components is necessary for studying biological cells, atmospheric behaviour, and numerous other organic phenomena [19]. A spectrophotometer is an instrument used to the intensity of light absorbed after it passes through the biological sample. The device is limited by uncertainties on the order of about 0.1 percent. Changing the spectrophotometer's structure at lower uncertainties helps to overcome the problems associated with its uncertainty [18].

The spectrometer may be held at an explicit wavelength, with repeated measurements made, while ensuring that the beam's geometry remains the same. For a precise outcome, the analyzed beam must be largely collimated, as with a conventional laser. Isolated light must be reduced and an integrating sphere utilized to diffuse incident radiation (light) and negate beam shifts. A calibrated spectrophotometer may also be used to investigate linearity and to analyze isolated light [18]. Several objects do not transmit light completely but absorb some of the electromagnetic radiation, convert it to heat, and reduce the amount of radiation transferred through the sample.

2.1.1.2 Absorptance Measurement

Absorptance is typically deduced from transmission measurements and not measured directly with appropriate rectifications for reflection losses. If refraction is known, these modifications are calculated from the Fresnel equations [18]. This method is not feasible for a medium with negligible absorption. Consequently, laser calorimetric measurements are performed to measure the absorptance directly [18].

2.1.1.3 Reflectance Measurement

Characterizing the occurrence of any material includes measuring the diffuse and specular reflectance. Different methods and instruments may be applied for reflectance, including reflectometers and integrating spheres. Reflectometers utilize mirrors to measure absolute specular reflectance, while many diffuse reflectance measurements involve integration spheres measurements made about some standard. However, absolute diffuse reflectance is determined through the double sphere method [18]. Other coherent sources and lasers are used to characterize smooth surfaces, while incoherent sources and specular reflection sources, such as tungsten-halogen sources, are generally employed for more diffuse specimens [18].

2.1.2 Cross-sectional Absorption

Tissue absorption may either have a destructive or therapeutic effect. Energy approaching from incident waves is moved into the tissue at every absorption event. There is no energy transmission between the tissue and incident radiation for non-absorbing situations. Light absorption by a tissue also plays a diagnostic role in medical imaging and tissue spectroscopy [18]. Absorption primarily occurs if the incoming photon's energy $h\upsilon$ is similar to the difference between energy levels ΔE in the molecule onto which radiation is incident [18].

$$\Delta E = h\upsilon . \qquad (2.6)$$

The molecule undertakes a quantized change in its vibrational state and charges separation because of absorption.

The following formalism could be developed for absorption. Figure 2.1 is showing the transmittance via a homogenous absorbing material. Consider a collimated beam of visible electromagnetic radiation with intensity I_o and wavelength λ passing through a homogeneous material with absorption coefficient μ_a (cm^{-1}). , light intensity I transmitted through the material of width l is denoted as:

$$I = I_o e^{-\mu l}, \tag{2.7}$$

where l is the photon path length.

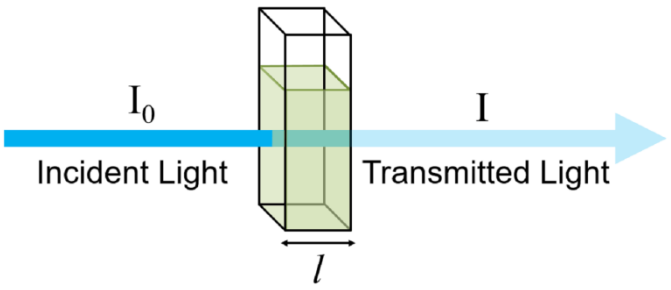

Figure 2.1: Light transmission via a homogenous absorbing material [61].

Mathematically, absorption is represented as [14]:

$$\mu_a = \rho_a \sigma_a, \tag{2.8}$$

where σ_a is the absorption cross-section(cm^2), and ρ_a the particle number density of the absorbers in the material expressed as:

$$\sigma_a = Q_a A, \qquad (2.9)$$

Here, Q_a and A are acknowledged as the absorption efficiency and the absorbing particle's geometrical area, respectively.

2.2.3 Cross-section for Scattering

We use the same analogy as in absorption, for scattering as

$$I = I_o e^{-\mu_s l}$$

l - is the photon path length.

Similarly, the scattering coefficient is described as:

$$\mu_s = \rho_s \sigma_s, \qquad (2.11)$$

σ_s - is the cross-section for scattering, and ρ_s the scatters' particle number density in the material is expressed by

$$\sigma_S = Q_S A, \qquad (2.12)$$

where Q_s denotes the scattering and A the geometrical area of the scattering particle, as shown in the figure on the next page:

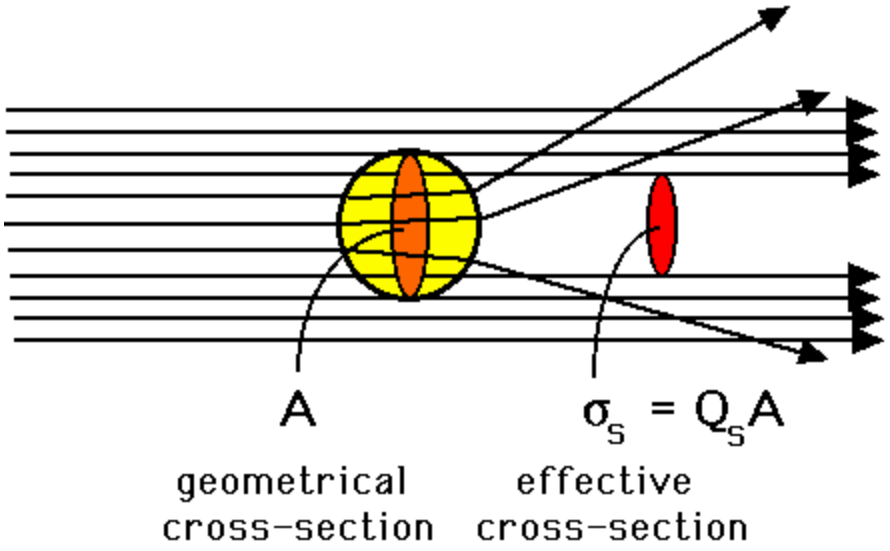

Figure 2.1: The cross-section for the scattering of a spherical particle [14]

2.2 Scattering by Particle

The study of light dispersed by particles has been valuable in various areas of science, from astronomy to cell biology and even atmospheric science. The amount of the radiation scattered depends on the wavelength of the incident radiation and applies to all types of electromagnetic radiation. The variation in the refractive indices of the two media also contributes to scattering [14]. The classical theory of electromagnetism explains scattering by particles as charges stimulated to vibrate by an oscillating electromagnetic field. Matter is usually electrically neutral but composed of numerous discrete charges. These fluctuating charges then radiate electromagnetic waves, which are dispersed. Coherent scattering occurs if the frequency of the secondary wave is roughly the same as the source frequency [20].

2.2.1 Single Scattering

Scattering is assumed to occur due to a coherent or irregular array of particles. For scattering by a regular (coherent) collection of particles, the nature of the incident light wave is essential, phases should be considered in contrast to scattering by incoherent arrays (for instance, tissue blood cells), and the phases are overlooked [24]. Molecules scatter light but not as particles [24]. Single scattering is observed only from a discrete, remote scattering particle on which energy from a definite basis is incident [24]. In theory, it is easier to estimate single

scattering occurrences than in practice, but multiple scattering is often viewed experimentally.

The scattering grade comprises the scattering particle's magnitude and shape, the geometry (angle), frequency, and polarization state of the incident radiation [24]. The scattering particle cross-section σ_s also determines the overall intensity or power of energy scattered by a particle, and likewise, the total power absorbed by the particle is determined by the absorption cross-section σ_a. The extinction cross-section (the area that is increased by electromagnetic waves irradiance incident on an object) provides the total radiant flux absorbed and scattered by the object and is then defined as:

$$\sigma_{ext} = \sigma_s + \sigma_a \qquad (2.13)$$

For this outcome, we presume that the incident radiation is moderately large in magnitude in contrast with the magnitude of the particle, gratified by the idea of plane waves, which is normally the basis for incident light in scattering experiments.

To examine the extinction cross-section, measurements of the spread of the energy slab of N similar scattering particles for every unit volume may be carried out [24]. The association between transmitted radiation and incident radiation is given by [24]:

$$I(h) = I_o e^{-N\sigma_{ext} l}, \qquad (2.14)$$

l is the slab thickness and is on condition that multiple scattering is ignored. These measurements of transmission present the extinction coefficients exclusively. Supplementary measurements are required for separate scattering and absorption cross-sections [24]. The above equation (2.14) entails that particles in the slab be similar, and to consider for comprehensive form in which there are variances between particles, $N\sigma_{ext}$ is substituted by

$$\sum_j N_j \sigma_{ext,j}, \qquad (2.15)$$

where j signifies all parameters apprehending one particle from another.

The following graph (Figure 2.6) illustrates the scattering quantity produced by particles of different radii through the Rayleigh-Gans estimate.

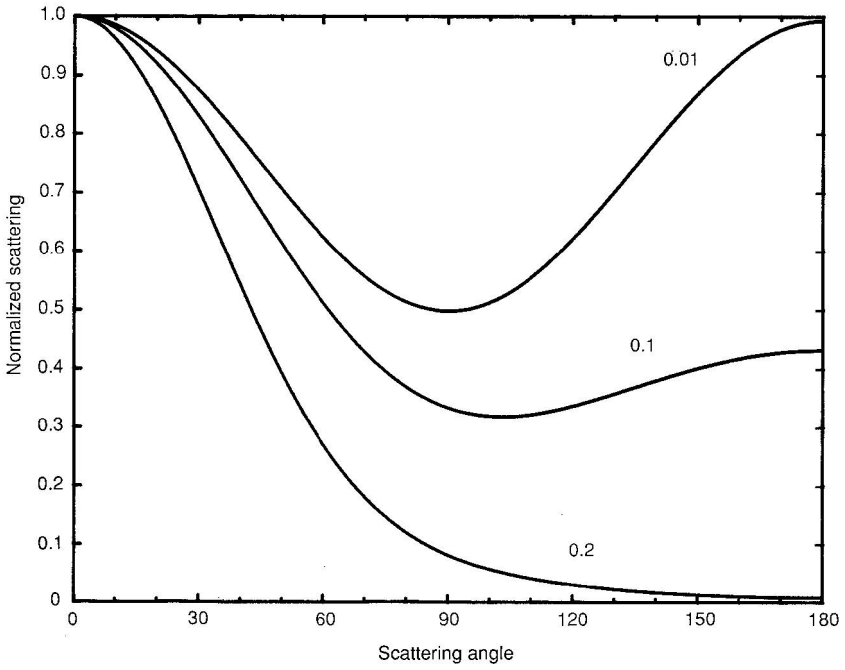

Figure 2.2: Unpolarized visible light scattering by spheres of radii 0.01, 0.1 and 0.2 μm [24]

It is explicit that a tiny sphere, of order 0.2 **μm**, may scatter light firmly in the forward direction. The most straightforward particle from which scattering is explained is an isotropic, homogenous sphere.

Various models and theories, such as Mie and Rayleigh, define the scattering of light. One of the frequently utilized theories, Mie theory, clarifies the scattering radiation due to spherical particles with the homogenous magnitude or greater than the wavelength of incident electromagnetic radiation. Rayleigh's theory is encompassed in Mie's theory but is required only as the scatter's magnitude approaches zero. Mie theory functions are applied solely to spherical particles. Mie theory functions are applied strictly to spherical particles and break down with irregularly shaped particles or molecules scattering [24]. Moreover, the Mie theory

functions are better suited for computing forward scattering than backscattering, making it ideal for tissue optics [24].

Any spherically symmetric particle induces a scattered field of the same form as that of a homogenous sphere; the scattering coefficients are the solitary thing that varies. Contrasting spherical particles incorporate consistently multi-layered and coated spheres. These particles might be amended by applying Bessel purposes to define their absorption or scattering properties [24].

Scattering by spheres and circular cylinders is impartially similar, with associated Bessel purposes [24]. Nevertheless, an immensely elongated cylinder may not have a limited volume and, therefore, the field scattered varies from that of a finite sphere. There is no precise theory for scattering by finite cylinders. However, approximations might be made by disregarding the end cylinder effects, with a significant ratio to their diameter. The geometry of the circumstances varies between the sphere and cylinder in that the scattering for cylinders depends on the incident plane wave polarization [24].

2.2.2 Computational Methods

complicated method to comprehend. Purcell-Pennypacker technique is a computational execution of Green's function and is more straightforward to function with mathematically than the T-matrix technique. A particle is estimated by N lattice, frequently isotropic and identical dipoles, each likened to the incident radiation wavelength. The dipoles are eager by all the other dipoles and incident fields and, therefore, abandon a collective of linear equations of 3 N at every dipole. Matrix of $3N \times 3N$ coefficient may be utilized and inverted to calculate scattering for various directions. This technique is restricted in that the computer's quantity of storage may be excessive [24].

2.2.3 The Radiative Transfer Equation

Analytical techniques of multiple scattering become too complex when working with media containing scattering core's arbitrary distribution. The radiative transfer model defines light propagation via tissue applying basic electromagnetic philosophy [24]. Tissue might be treated arbitrarily as wave properties like polarization and interference. However, radiative transfer philosophy's basic assumption is the unique radiation examination through the medium [24].

The radiative transfer equation (RTE) defines the alteration of radiation radiance $I(r,t,s)$ at location **r** in direction s, with c Light speed in the medium, Absorption coefficient μ_a, Scattering coefficient μ_s, Phase function $f(s,s')$, and Radiation source $q(r,t,s)$ as follows:

$$\frac{1}{c}\frac{\partial I(r,t,s)}{\partial t} + s.\nabla I(r,t,s) + (\mu_a+\mu_s)I(r,t,s) = \mu_s \int_{4\pi} f(s,s')I(r,t,s')d^2s' + q(r,t,s), \qquad (2.16)$$

The radiation illumination $I(r,t,s)$ is the radiation transfer per unit time per solid angle d^2s via unit time t and position r [24]. Combining $I(r,t,s)$ over every angle provides the flux Γ through a unit area **n**

$$\Gamma(r,t) = \int_{4\pi} I(r,t,s)s.nd^2s. \quad (2.17)$$

The radiative transfer equation acquired by examining the balance in radiant energy in a random volume tissue element is an equation relating the variation of energy illumination in time (first factor) to a variation in energy flow (second factor), loss because of absorption and scattering (third factor), improvement because of scattering sources (fourth factor), and gain because of radiation sources (fifth factor) [24]. Solutions of the radiative transfer equation may be found for instances with an isotropic scattering in modest geometries [24].

2.3.4.1 Diffusion Approximation

In numerous organic tissues $\mu_s \rangle\rangle \mu_a$, simplifications may reduce the radiative transport equation to the diffusion equation [18].

$$\frac{1}{c}\frac{\partial\phi(\vec{r},t)}{\partial t} + \mu_a\phi(\vec{r},t) - \nabla\cdot[D\nabla\phi(\vec{r},t)] = s(\vec{r},t) \quad (2.18)$$

$$D = \frac{1}{3(\mu_a + \mu_s^{'})}$$

$\phi =$ Rate of fluence (flow of energy at all degrees per unit normal area per unit time)

$D =$ Diffusion constant

2.4 Beer-Lambert Law

The Beer-Lambert law describes the relationship between the number of absorbing species within that sample, the intensity of light transmitted through an absorbing sample, the path length through which the light travels and the sample thickness. In Figure 2.4 [18], this association is defined mathematically.

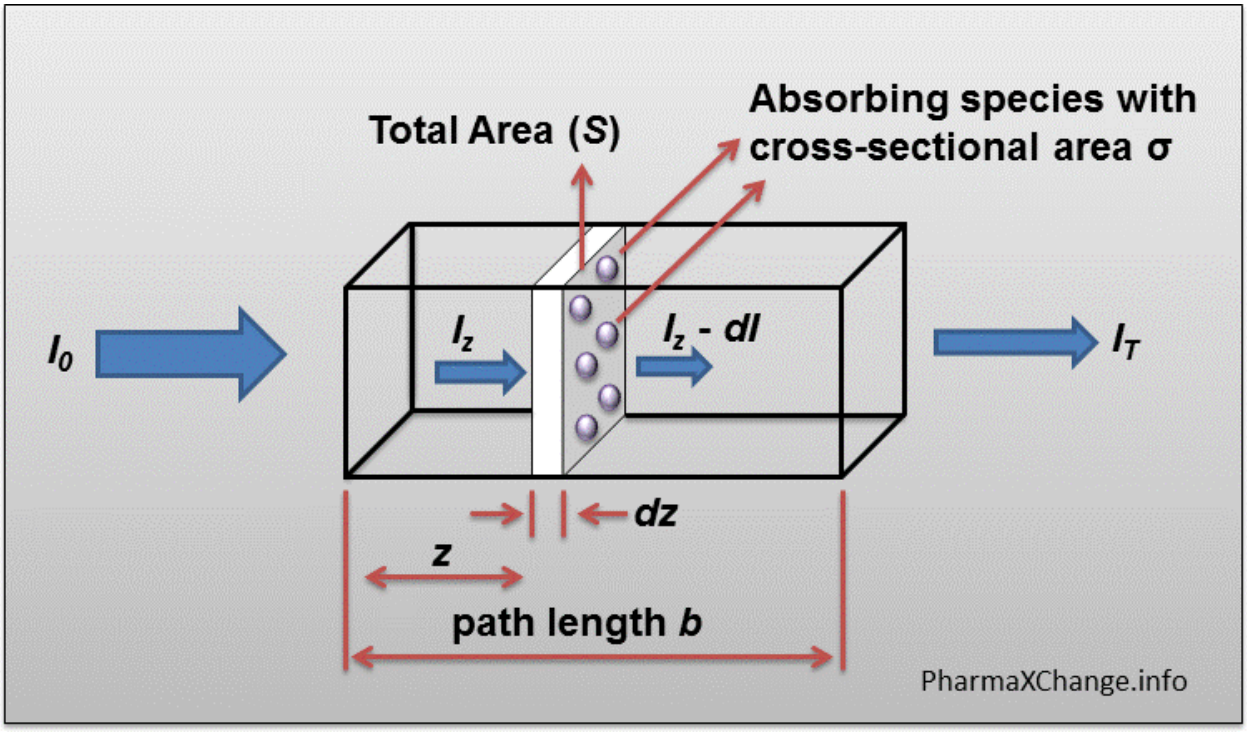

Figure 2.3: A diagram constituting a sample thickness b to derive the Beer-Lambert law [18]

For a monochromatic light with incident intensity I_o, and transmitted intensity I_T, and small slab thickness dz, the photons absorb through path length b because of the *n* molecules/ cm^3. The number of molecules existing in the infinitesimal slab is, therefore:

$$n \times S \times dz, \tag{2.19}$$

and the comprehensive fractional area on the slab to the absorbers is defined as

$$(n \times S \times dz) \times (\sigma/S) = \sigma \times n \times dz, \tag{2.20}$$

Given that every absorbing molecule has a cross-sectional area σ [34], the radiation absorbed by the tiny slab molecules is dI. Therefore, the small proportion of radiation absorbed is dI/I_z. Since the total fractional area absorbing molecules for the total absorption happen in the slab, therefore:

$$\frac{dI}{I_z} = -\sigma \times n \times dz \tag{2.21}$$

$$\Rightarrow \int_0^b \frac{dI}{I_z} = -\int_0^b \sigma \times n \times dz$$

$$\Rightarrow -\ln\left(\frac{I_z}{I_0}\right) = \sigma \times n \times b, \tag{2.22}$$

The above expression can be rewritten as:

$$-\log\left(\frac{I_z}{I_0}\right) = A = \varepsilon \times b \times c,$$

The absorbance is identified as the wavelength reliant on the molar absorptivity coefficient and the absorber concentration [34]. A tissue through a turbid medium with absorption coefficient is not merely absorbing. The Beer-Lambert law may still be utilized to a reasonably accurate degree to comprehend the distribution of light within tissue, given that the sample tissue reduces the number of scattering proceedings, which approximately simulates an entirely absorbing medium [34].

2.5 Interaction of Light Tissue

2.5.1 Transport Coefficients

Once an incident photon propagates over a short distance ds in a tissue, the likelihood of scattering over this distance is $\mu_s ds,$ [22], likewise the probability of absorption follow the same pattern. Mean free pathway for an absorption occurrence is $\frac{1}{\mu_a}$ and $\frac{1}{\mu_s}$ for a scattering occurrence.

In a turbid medium, it is typical to define the sum of the scattering and absorption coefficients as the total transport or attenuation coefficient μ_t [22]:

$$\mu_t = \mu_a + \mu_s \tag{2.24}$$

2.5.2 Penetration Depth

The penetration depth of collimated beam is described as the mean free path for scattering or absorption, which precisely is the mean distance into a tissue which the photon travels before absorption or scattering occurs [22]. It is expressed as the reciprocal of the attenuation coefficient.

$$\delta = \frac{1}{\mu_t} \tag{2.25}$$

2.5.3 Attenuation of Light

It is hard to precisely measure the collimated light transmission, as transmission measurements are probable to consist of scattered light [22]. Transmitted light via the air-tissue interface will endure absorption or scattering at one point in the tissue. The melanin absorption coefficient in tissue decreases as the wavelength of the incident light increases, whereas the absorption by blood depends on the wavelength and the oxygenation of the blood. At specific wavelengths, the absorption of deoxygenated and oxygenated blood is equal, as demonstrated by the points of intersection in Figure 2.5.

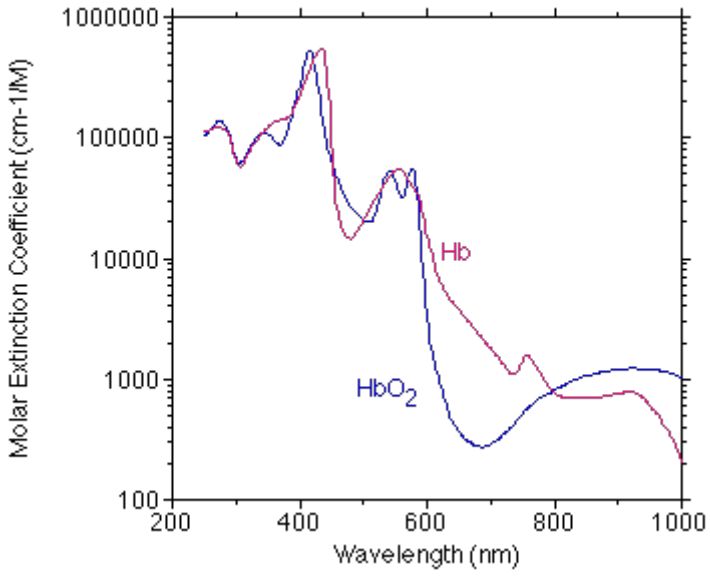

Figure 2.4: Absorption coefficient of oxy-and deoxyhemoglobin as a function of wavelength [15]

Proteins and amino acids become the primary absorbers at wavelengths in the UV spectral range, and water is the most highly absorbing of the chromophores at Infrared (IR) wavelengths. At wavelengths above 1.4 μm, the scattering in tissue becomes insignificant compared to the absorption [22]. This wavelength is in the spectrum's infrared range. Hence, the primary cause for the attenuation in this range is water. The absorption coefficient (and, thus, the transport coefficient) of the tissue may then be estimated by the absorption coefficient of water, considering the water concentration in that tissue. Changes in the temperature of the water can also affect its absorption characteristics [22].

2.5.4 Lasers in Cancer Treatment

Laser therapy utilizes high-intensity light to manage cancer and other diseases. It is used to destroy pre-cancerous growths or shrink tumors. It is typically used to manage superficial cancers like basal cell skin cancer and the very primary stages of some cancers, such as cervical, penile, vaginal, vulvar, and non-small cell lung cancer [35].

Laser therapy may be soley performed, but it is mostly combined with other treatments, such as surgery, chemotherapy, or radiation therapy. It is carried out through an adjustable endoscope (a narrow, lighted tube utilized to observe tissues within the body). The endoscope is integrated with optical fibers (thin fibers that transfer light). The latter is incorporated through inception in the body, like the vagina, nose, mouth, or anus [35].

Photocoagulation of Laser-induced interstitial thermotherapy (LITT) is also a cancer treatment comparable to hyperthermia. It is used for treating tumors or killing cancer cells by heat. LITT involves a Laser light at the tip of an optical fiber incorporated into a tumor. The light increases the tumor cell's temperature destroying and damaging the cells [35].

Photodynamic therapy (PDT) is a different type of cancer treatment that utilizes lasers. In PDT, a definite drug, called a photosensitizing or photosensitizer agent, is inserted into a patient and consumed by cells over the patient's entire body. After some days, Laser light is utilized to stimulate the agent and abolish the cancer cells.

Three kinds of lasers are used for cancer treatment: Carbon dioxide (CO_2) lasers, Argon lasers, and neodymium: yttrium-aluminum-garnet (Nd: YAG lasers) [21]. CO_2 and argon lasers may cut the skin's surface without going into deeper layers. Thus, they are useful for treating superficial cancers, such as skin cancer. In contrast, the Nd: YAG laser is usually applied via an endoscope to treat internal organs, such as the esophagus, uterus, and colon [35]. Nd: YAG laser light may also propagate via optical fibers into exact parts of the body during LITT.

2.5.4.2 Overview of PDT

A particular drug called photosensitizing agent is introduced into the bloodstream. The photosensitizing agent stays longer in or near cancerous tissues than normal tissues and it is absorbed by the body tissues with time. Irradiation of the body with light of a particular frequency activates this chemical agent, causing a chemical reaction which consequently destroys the cancerous cells [35]. The timing of exposed light should be carefully monitored for the chemical agent to evacuate surrounding cancerous cells from the healthy cells [35].

The major disadvantage of PDT is that photosensitizing agents may leave the human body vastly sensitive to visible light, prompting sunburn-like side effects even after little exposure. The patient might sometimes need to wait for weeks until the chemical agent entirely evacuates the body.

PDT is at times employed to treat cancers and pre-cancers of the esophagus. Other lung cancer types may also be treated with PDT, using endoscopes [35]. Different photosensitizing drugs and laser types that can be more effective and safe are currently being looked at by researchers [35]. The agent employed in PDT is generally activated by near-infrared or visible

light, permitting specific organic effects in tissues or cells. These organic effects may be used to treat particular kinds of tumors. Interactions between the tissue and light are both photomechanical and photothermal [35].

2.5.4.3 PDT Mechanisms

The agent (photosensitiser) is primarily in its ground state (S_0) and gets excited to state (S_1) through the photon absorption of suitable wavelength (as shown in Figure 2.6). A photon with the same wavelength might then be emitted from the excited photosensitiser to go back to state S_0, cross to a triplet state of energy T_1. The state (T_1) is comparatively longer existed (~ μ_s) than the state S_1 as the transition to S_0 (from T_1) is prohibited by quantum mechanics. During this period, the triplet state may interact with the organic tissue in which the agent is positioned. This relation may be instantaneous with an organic molecule (type one interactions), or T_1 may interchange energy with triplet molecule on the ground state (type two interactions). Type two interactions create singlet O_2 which react promptly with organic molecules, have lifetime less than $1\mu_s$ and disperse through a much lesser distance than μm inside the tissue [36]. The organic effect that arises from creation of O_2 is, thus, confined to the area where the photosensitizer is present. The photosensitiser will ultimately reclaim its primary ground state and will either be killed significantly by exchange between the photosensitizing agent and light, or indirectly via melting of the O_2. Numerous photosensitising agents presently employed for PDT are confined on the cell membranes, like lysosomes and mitochondria. The restricting factor of this technique is that an adequate oxygen level is needed in the tissue for organic effects to take place. However, numerous tumours have low oxygenation levels. Figure 2.6, demonstrations cell death mechanisms in PDT [36].

Figure 2. 5: **Mechanism of cell death and the electronic states in PDT** [36]

2.5.4.4 Photosensitisers

Photosensitisers require a precise photon's wavelength that may infiltrate the needed depth in tissue [37]. These agents also need to be highly confined to a tissue site to ensure organic effects simply in the area needing treatment [37]. Several of the other deliberations to be prepared are that the photosensitisers requirement must be non-toxic, reasonably simple to produce, and cost-effective. Various photosensitizing agents are employed, depending on the tumor's location and are selected according to absorption spectra. The drug photofrin is used as a photosensitizer for wavelengths close to 400 nm and greatly inadequate photons absorption of wavelength near 630 nm [37].

2.5.4.5 Light in PDT

The energy needed in PDT is great, likened to radiotherapy, where the dosage absorbed for hard tumors is about $0.05\ \mathrm{J.cm^{-3}}$. In PDT, the standard absorbed energy density is $100\ \mathrm{J.cm^{-3}}$. Given that light in the wavelength range (400 – 700 nm) is appropriate in PDT, it turns out to be hard to illuminate adequately a tissue volume at a vital depth [37]. This absorption and scattering lead light to diffuse at times close to millimeters once it passes a tissue. The absorption and scattering inside a tissue decline as the wavelength surges near the infrared and visible range and since the hemoglobin drops quickly at wavelengths beyond approximately 600 nm [37]. The initial absorption summit of water is attained at more than 900 nm. It has been observed that tissue necrosis occurs solely in areas where PDT product dosage is beyond a specific threshold value. The dosage's efficiency is proportional to the extent of light incident on the affected tissue [37]. The concentration for threshold is attained with adequate PDT dosage, the light combination, intrinsic oxygen, and photosensitizing agent [37]. The O_2 manufactured may either destroy cells by necrosis (not controlled cell death) or apoptosis (encoded cell death).

PDT does not disturb DNA, so the consequences are direct instead of genetic, unlike particular drugs employed in chemotherapy or radiotherapy. Even if there is a reliance on the type of photosensitizing agent, various cells' reaction to PDT is not significantly varied. If the

photosensitizing agent exists in cells coating blood vessels, the cells may be destroyed, leading to thrombus formation, causing a cease in the area's blood flow to cease. The death cell may activate vascular reactions in the body and even result in a vascular shutdown.

Most of the present PDT treatments are high doses compared to chemotherapy or radiotherapy, where repeated small dosages are given to the patient over a period. The current investigation in PDT is applying the dose quantity in metronomic PDT (mPDT). In this treatment, both dosages of photosensitizing agent and light are given minor doses continuously or repeatedly over a lengthier duration [37].

2.6 Tissue Phantoms

Optical phantoms are tissue-simulating objects used to mimic light propagation in living tissue. They are designed with absorption and scattering properties matching living human and animal tissues [38]. Optical tissue phantoms can be used for testing systems in development, calibration and quality control of existing systems, and inter-system and inter-lab comparisons. To obtain quantitative information, steady-state optical measurements with phantoms can be an essential step for inaccurate calibration. Solid phantoms based on optical-grade polymers, absorbers, and scatters offer long-term stability and reproducible optical properties [38].

Optical properties determination of tissue is fundamental for laser usage in diagnostic or therapeutic techniques. Phantoms may be employed to test the apparatus set-up and effectiveness, design, and equipment calibration. In optical imaging, phantoms may be utilized to compare and determine the dissimilarities in polarization states of visible light, distinguish between various types of phantom tissues, and detect a tissue's constituent concentrations [38]. The interaction between the incident light and the phantom tissue components may explain Mie's theory, taking the medium's scatters as non-interaction, isolated spheres. The kind of material in which scatterers and absorbers are confined may be solid or liquid [39]. Phantoms, which are liquids, are simpler to make compared with solid.

Nevertheless, solid phantoms are appropriate for mimicking tissues with complex structures, such as multi-layered tissue [39].

Methods made based on tissue models have been utilized for oxygenation in blood and non-invasively monitor glucose. Phantom tissues are significantly employed in research associated with photothermal coagulation, PDT, and laser ablation [13, 27]. The non-invasive natural surroundings of numerous biomedical techniques are, in certain instances, the consequence of work done on simulating the phantoms of a tissue. It is exciting to explore this research field since the medical diagnosis is better managed noninvasively. One such diagnostic technique is discovering breast cancer at the primary stage by light transillumination. It avoids the requirement for mammography of X-ray, which is possibly harmful. The breast tissue is greatly scattering, and the method needed to be enhanced upon by utilizing tissue phantoms to mimic the various scattering inside the breast. Numerous experiments support turbid media to define the real optical properties of the human's breast *in vivo* [26].

Various techniques used to regulate the suitable optical tissue properties involve frequency-domain diffuse reflectance, integrating sphere, optoacoustic, and time-domain diffuse-reflectance [27]. The advantages and disadvantages vary in utilizing the suitable technique, depending on the circumstance or the particular tissue geometry being examined [27].

Optical tissue properties determination is essential for light application in either diagnostic or therapeutic techniques. Phantom tissue is a synthetic or virtual tissue made to model light transportation and mimic human tissue optical properties. The absorption and scattering coefficients like the anisotropy may be obtained for tissues in a human body from an attentively manufactured mimicking phantom [27].

The optical tissue properties, once deduced, may be employed to estimate energy deposition and light scattering on a tissue. In the past, numerous evaluations have established that these optical properties are *ex vivo* and assume that there is uncertainty about this method, as the organic tissue of an individual differs in water and blood content. Chromophores will affect

attenuation in those tissues, and differences in their levels, have to be accounted for. Understanding the optical properties of the tissue at appropriate wavelengths is more significant than knowing their actual values. The tissue optical properties behavior, the water of the tissue, blood, and fat content may be scrutinised as managed parameters. Employing tissue simulating material to regulate these parameters is more feasible than experiments within or with living organisms [28].

2.6.1 Continuous and Discrete Particle Tissue Models

Tissues typically comprising inhomogeneous systems with extensive size arbitrarily spread throughout the tissue's medium. The tissue is frequently designed either as a discrete ensemble of chromophores or scatterers. The model employed rests on the organizational complexity of the degree of light tissue scattering. Blood is a great biological system example that suits the model where the particles are dispersed and discrete. Numerous biological media are designed as spherical, non-interacting particles as numerous microorganisms and cells are approximately spherical in structure, for example, blood [29]. A non-interacting system, Mie theory, may be employed since spherical particles are the easiest tissue model. Mie theory may be utilized to describe spherical particles and also cylindrical particles. Fibre structures and connective tissue may be modeled by estimating them to be lengthy cylinders, and the single homogenous cylinders or multi-layered cylinders are scattered by employing Mie theory [29].

2.6.1.1 Refractive and Absorption Index

Cell organelles, cell nuclei, tissue fibres, and melanin particles are the models accountable for numerous refractive index variations inside a tissue. The Gladstone and Dale law [29] may be utilized to determine the interstitial medium refractive index, organic tissue, and relative components. The particle refractive index summarizes the mean index variation and the background index. In contrast, the regular background index describes the refractive indices' weighted average of the cytoplasm - the cell ground substance and the interstitial liquid. The

cell average refractive index is approximately 1.42, and the cytoplasm refractive index is about 1.38 [29].

Absorption by tissues is insignificantly lesser in the visible electromagnetic spectrum, with only melanin, hemoglobin, and other chromophores absorbing lesser light in this region. Most absorption is due to water molecules in tissue in the electromagnetic spectrum's infrared range, and protein bands are primarily absorbed in ultraviolet wavelengths [29].

2.6.1.2 Anisotropy of a Tissue

Anisotropy is predominant with the forward scattering of the collimated light in organic tissues. When a photon is scattered by a particle and its trajectory is deflected by scattering angle (θ), the component of the new path is aligned in the forward direction as cos (θ) [28]. The mean value of the average scattering angle cos (θ) is called the anisotropic factor (g), Illustrated mathematically as follows;

$$g = < \cos\theta > \tag{2.26}$$

Numerous organic tissues are optically birefringent and anisotropic. For instance, tendons frequently contain parallel, heavily filled collagen fibers conducting parallel to solitarily axes, making them vastly birefringent like a tissue. For biological systems with enormous diameters, the birefringence proceeds to zero. Birefringence values of tendon, skin, and muscle are of the order of 10^{-3} [29]. Cartilage and birefringence of the skin are not constantly dispersed. In tendons in their orientation and amplitude, fibres of collagen in cartilage and skin do not have constant densities as tendons. The method permitting the exact birefringence measurement in turbid tissues is called polarization-sensitive optical coherence tomography (PS-OCT). PS OCT methods are usually functional in dermatology, dentistry, and ophthalmology [29]. Variations in birefringence may indicate beneficial alterations in tissue, like photothermal injury at the time of laser surgery that varies the birefringence in subsurface tissue [29].

2.6.1.3 Tissue Components' Volume Fraction

The packing density or volume fraction signifies the tissue volume taken by its elemental particles. The volume fraction of a phantom or tissue sample influences optical properties like refractive index and anisotropy [29]. The tissue sample volume fraction interpretation, like a phantom, may be created from a thin slice of the prototype. However, these solutions may be deceptive as the spread of scatterers is probably entirely irregular throughout the sample [29]. Nevertheless, the usage of a dissimilar slice can lead to entirely contrasting results. The scatterers' volume fraction in human tissue like a cornea and a muscle varies between 20% and 40%. In a blood cubic millimeter, there occur $(2-3)\times10^5$ platelets, $(4-5)\times10^6$ erythrocytes, and $(4-9)\times10^3$ leukocytes. Sixty percent of blood is generally plasma, whereas erythrocytes take the remaining. The particles' arrangement ensures sufficient distance amongst scattering particles proportional to their size [29].

2.6.2 Tissue Phantoms Construction

A characteristic phantom entails a host of diluents/medium, an absorbing medium, and a scattering medium. The objective is to fabricate a mixture of the relevant quantities of scatterers, diluents, and absorbers to simulate the required tissue's optical properties. Properties to be regulated by phantom measurements comprise the absorption coefficient μ_a , anisotropy g , and scattering coefficient μ_s . Optical properties for soft tissues general ranges are $g=0.9$, $\mu_s \varepsilon [0.2; 400]\mathrm{cm}^{-1}$ and $\mu_a \varepsilon [0.5; 5.0]\mathrm{cm}^{-1}$ for both NIR and visible wavelengths. Hard phantoms are typically created from transparent hosts, like agar, gelatin, or even wax, that characteristically scatter visible light. The tissue simulation with composite geometries may be achieved using inhomogeneities at the appropriate sites and layered phantoms. These optical phantoms must mimic optical properties in tissue at the required wavelengths. However, some optical tissue phantoms have more accurate properties compared to a wide range of wavelengths [14].

In accordance with Tuchin [14], a real tissue phantom must satisfy the subsequent necessities:

- It must sample the optical and geometry parameters of the phantom tissue appropriate for the transport of visible light [14].
- Phantom tissue components should be harmonious with one another for spectroscopic properties and chemical stability [14].
- The appropriate radiation transport parameters should be predictable and reproducible from the sample's composition [14].
- The phantom physical parameters should be temporally steady (aging, diffusion, evaporation) and not dependent on the environment [14].
- The phantom creation must permit inhomogeneous tissue geometries demonstrated by moulding methods or stacking phantom slabs [14].
- The sample must be quick, safe and simple to make [14].

Based on the discrete particle tissue model, optical tissue properties' real values are over a wide range of wavelengths. Mie theory may, thus, be used to determine scattering and absorption by the particles inside the tissue [14]. Several appropriate particle parameters needed for the Mie theory application include the compounded refractive index.

$$n_s(\lambda_0) = n_s^{'}(\lambda_0) + in_s^{''}(\lambda_0), \qquad (2.27)$$

The index of refraction for the host material n_0 and the scatterers' comparative refractive index and host $m = \frac{n_s}{n_0}$, whereby λ_0 is the wavelength in the vacuum and the compound refractive index imaginary part is accountable for the losses in visible light because of absorption. The absorption and scattering coefficients may also be established using Ricatti-Bessel functions [14] in equations for the Mie coefficients. The distance d_s (mean) among scattering particles may be articulated concerning the dimensionless volume fraction of the scatterers c_s and the scatterers' a_s radius by,

$$d_s = \frac{2a_s}{\sqrt[3]{c_s}} \qquad (2.28)$$

Mie theory functions well with shaped particles, like spheres, and when the particles are scattered and have a radius on the same scale as incident light [14]. This is normally the situation with materials employed for the fabrication of tissue phantoms.
Wavelengths with lower values are likely to be dispersed in organic tissue, with a higher anisotropy. It is best to make a mixture of bigger particles that contribute a higher anisotropy and tiny particles that scatter wavelengths with lower values to mimic an organic tissue [31].

2.6.2.1 Host Media

Several phantom matrix possibilities to hold absorbers and scatterers comprise:

- Polyacrylamide gel
- Agar/gel matrix
- Room temperature vulcanizing silicone
- Aqueous solutions
- Polyurethane/polyester resin.

2.6.2.2 Scattering Media

In the liquid phantom fabrication, the familiar scattering materials are fat emulsions which are intravenous, like Liposyn, Intralipid, and Intralipid. These particular drugs comprise glycerol, egg phospholipids, and soya bean oil and signify droplets of spherical fat suspended in water. Hard phantoms of Intralipid undertake a considerable variation in scattering coefficient via a minor difference in scatterer concentration. Furthermore, it has been established that temperature variations during solid phantoms fabrication may affect the induced interactions with agar and scatterers [31].

Scatterers mostly utilized in hard phantoms consist of polystyrene latex spheres with a diameter of approximately a few micrometers. Al_2O_3 and TiO_2 spherical particles with a diameter ranging from 20 nm to 70 nm are also frequently utilized as a suspension in gel or an aqueous solution dispersing light [31]. Microspheres of quartz glass are challenging to

obtain. However, these particles may behave as scatterers with a diameter of approximately 250 nm. Al_2O_3 Polystyrene does not melt in water (hydrophilic), making them perfect for application in solid phantoms with a base material of gelatin or agar. Sonication is normally taken out on gels that are warm, to which the scattering particles are increased to avoid sedimentation of particles while the host material is yet non-viscous [31].

2.6.2.3 Absorbing Media

The absorption of light in a tissue is demonstrated based on absorption coefficient determined directly and indirectly in phantom tissues. Some natural dyes (like india ink) [32], are applied mainly as absorbing media in tissue phantoms on condition of their absorbance at various wavelengths and ability to dissolve in the host material. Regular stains applied in microscopy absorb light in the NIR and visible electromagnetic spectrum regions are appropriate for tissue-like simulations [31].

2.7 Optical Coherence Tomography

Some part of a light incident on organic tissue is redirected from refraction index mismatches. Amplitude signifies scale of mismatch and depth of mismatch is indicated by timing. Optical coherence tomography is exceptional for microstructure mapping of a tissue (tens of microns scale). That ability exists in robust, modest structures [23].

Various A-scans (50-500/mm is characteristic) are collected when a beam of light is scanned horizontally across the sample and:

- This provides two-dimensional image or B-scan.
- The data that is raw from one A—scan is demodulated to measure the amplitude and signal phase.

Many tissues have numerous refraction indexes that mismatch. The demodulated A-scan amplitude is approximately an extent-resolved signal of the tissue backscattering properties [23].

2.8 Fourier Domain OCT

It is necessary for actual tissues to think through the truth that between reflected waves from scatterers of tissue, there will be interference. The common interference of these scatterers happens nearby z = 0. Usually, this interference's size is greatly more fragile than the actual signal since the signal's term is weighted with robust reflectance amplitude [23].

2.8.1: Advantages of Fourier Domain Optical Coherence Tomography (FDOCT)

Speed of fast acquisition is one of the advantages**.** There are no scanning elements required to obtain a-scan data**,** every a-scan is data obtained in solitary linear sensor array exposure. Another advantage is increase of SNR. Every N a-scan knowledge is obtained at once, for equal imaging speed to each element and is shown N times longer. The SNR rises by an N square root for shot noise restricted operation [23].

2.8.2 Disadvantages of Fourier Domain Optical Coherence Tomography (FDOCT)

SNR decreases with depth. This is one of the disadvantages. Restriction of imaging depth by the spectrometer resolution and added processing of data are the other challenges [22]. FDOCT should interpolate spectrum obtained as a wavelength function into v function, then after Fourier transform data before displaying. Furthermore, there are technology restrictions and arrays of a detector that are louder than solitary element photo detectors [23].

2.9 Diffuse Optical Tomography

The modality of imaging in which dimensionally unvarying optical properties are deduced from fluence of surface measurements is named diffuse optical tomography.

Advantages of diffuse optical tomography are [23]:

Information of functionality:

$\mu_a \Rightarrow Hb, HbO_2, H_2O$, concentration of fat

$\mu_s \Rightarrow$ Information of structure

Affordable, "portable" (compared to CT, MRI)

Disadvantages of diffuse optical tomography are:

Resolution is low by several millimeters and reconstruction is very challenging, for instance, tumor dimension and optical properties need to be determined.

2.9.1 Instrumentation

Diffuse optical tomography has several sources and several sensors in numerous geometries, like slab, ring, and array [23]. Continuous wave system source radiates light at a uniform intensity into the tissue and back scattered and transmitted light intensities are computed. In order to prevent interferences from the environment, the amplitude may be modulated by few KHz. This system mentioned above measures the reduction of the detected light intensity in comparison with the emitted light intensity. The continuous wave technology is vastly used in neuroimaging research because it is cost effective and is easy use [60].

2.9.2 Probabilistic Photon Path

The route from a source taken by a photon is not known but its probability is known [23]. Given a detector and a source, photon behavior whilst traveling inside or within a turbid medium such as human tissue can be ballistic, diffusion or scattering, quasi-coherent or backscattering. In ballistic behavior, the photons travel inside a medium without the scattering process taking place, getting to the detector in a short duration, since they travel by the shortest distance. The propagation direction is the same as that of emitted light. In quasi-coherent behavior, the photons propagate in the same path as the light emitted, reaching the detector rapidly. Nevertheless, the path zigzags the obstacles. In scattering or diffusion behavior, the photons suffer a lot of missing information, processing and scattering from the emitted light, getting to the detector later than the ballistic or quasi-coherent, since

they use a longer trajectory. The photons in backscattering return in the same trajectory as the emitted light, since the travel angle is varied, without reaching the detector [60].

2.9.3 Inverse Problem of Diffuse Optical Tomography

There is no precise analytic solution that exists, although some can be simplified. There are characteristic approaches like back projection, which is filtered, taking into consideration probabilistic photons trajectory and iterative method [31]. Firstly, there is assumption of a primary set of coefficients of attenuation, compute forward problem (fluences). There is also alter guess, an attenuation coefficient relying on difference between measured and computed fluence [23].

2.10 Types of DOT Instruments

2.10.1 Diffuse Optical Tomography

Source Modulation

It includes:

- domain of the frequency (diffusion waves)
- Domain of a time (take advantage of varying routes of late and early photons)

The above domains can differentiate scattering and absorption.

- Steady state
- Measurement geometry
- Constrained with data of magnetic resonance imaging or free form
- Contrast improved or intrinsic contrast [23]

2.10.2 Bioluminescence

In bioluminescence, visible an electromagnetic wave is made by organic creatures. Creatures like earthworms, fireflies, fungi (normally green, red or yellow), and centipedes propagate visible light on land and at sea creatures like plankton, bacteria, jellies, fish (normally green or blue), and crustaceans emit electromagnetic wave [23]. It is of utmost significance to gather some information about two bioluminescence types, which are luciferase or luciferin reaction and fluorescent proteins. In luciferase or luciferin, chemical light production needs the energy of organisms, for example fireflies.

2.10.3 Luciferase or Luciferin Reaction

Luciferin is any material that radiates light as soon as it loses some electrons in the existence of luciferase, whereas luciferase is any enzyme that should exist to facilitate luciferin oxidation. There are numerous forms of luciferase and luciferin, but all these forms need the existence of adenosine triphosphate (ATP) and oxygen [23].

Luciferin + ATP ---> luciferin adenylate + PPi

Luciferin adenylate + O2 ---> ox luciferin + AMP + light

The reaction above is very efficient in light production from energy kept in ATP.

2.10.4 *In vivo* Use of Luc Reaction

Cells may be transfected by the sequence of genetic to make luciferase. This order may be merged beyond a promoter; luciferase will solely be created by the gene of curiosity if is being uttered. Bacteria that organically produce luciferin and luciferase may be presented into a host, for example to a track infection [23]. No extra process is required, apart from collecting visible electromagnetic wave from the bacteria using a light-proof box. Luciferin should be injected for those cells uttering luciferase. Also, ATP and oxygen must adequate for reaction to continue.

2.10.5 Fluorescent Proteins

In production of fluorescent proteins, cells may as well be transfected by the genetic order. Fluorescent protein is extensively used is a green one. However, their availability is from a blue to a red emission wavelength. External excitation light should be given [23].

2.10.6 Problem with Fluorescence

The animals are relatively extremely fluorescent; this makes detection of cells that are fluorescently labeled difficult [23].

2.10.7 Fluorescence Molecular Tomography

It may use values of diffuse optical tomography in order to gain three dimensional images [36]. It is very easy to use this technique in small mice than in human beings. Computed tomography is frequently supplemented to offer anatomical reference [23].

2.10.8 Port Wine Stain

It is a birthmark which appears as if somebody spilled wine on the human skin. Some children are born with port wine stain (PWS). On adults, PWS is purple or red in colour and may appear anywhere on the human body. PWS may, or may seldom show a critical deep lying condition [23].

Chapter 3

3.0 Experimental Details

This chapter contains all the information to recreate the experiment. The information entails details of the material used to perform the experiment and precise details of the techniques employed in the experiment.

3.1 Apparatus

3.1.1 Soy Agar Phantom

The Tryptic Soy agar powder (Sigma Aldrich, MO, USA) was employed as the base material for the fabrication of optical tissue phantoms. Agar is a matrix hydrogel material consisting of a network of hydrophilic polymers widely used to prepare phantoms for optical imaging and biophotonics applications in the medical field. It is a biologically and biochemically compatible material with intrinsic optical properties as soft tissue composition and structure [40].

3.1.2. Scattering and Absorbing Agents

Aluminum oxide (Al_2O_3) powder, with irregular spherical formulations, and black India ink, were added to control the scattering and absorbing properties of the Agar gel due to their high scattering coefficients, availability, and wider acceptability [41].

A digital balance (with 0.01g readability) measures the quantity of scatters and absorbers used in a sample. This balance was capable of precisely measuring these very same quantities.

3.2 Methodology

3.2.1 Recipe for phantom fabrication

The recipe to create the phantom samples was the same as described by Hartleb [31], considering the ease of preparation and the use of cost-effective, readily available equipment:

- Specified amounts of the Soy agar were dissolved in 100 ml deionized water with aluminum oxide and black ink.
- The mixture was heated to 40 ^{o}C and then continuously stirred (for the agar powder granules to dissolve and the Al_2O_3particles to be evenly distributed) until a temperature of about 96 ^{o}C - agar activation temperature.
- The mixture was steadily stirred until sufficiently cooled to room temperature, creating a homogenous solution.
- The mixture was covered with aluminum foil and placed in a refrigerator overnight to harden.
- Before solidification in the refrigerator, the agar formed a moderately firm gel.

  During the heating process, the sample temperature readings were taken with a Techgear TG732TK dual channel digital thermometer and red alcohol thermometer, modified to use a thermocouple across the beaker by a Velcro's backstrap. The temperature was measured with an accuracy of $\pm 5^{o}C$.

Figure 3.1 is a sample of the pure phantom (without scatters and absorbers) tissue from this study.

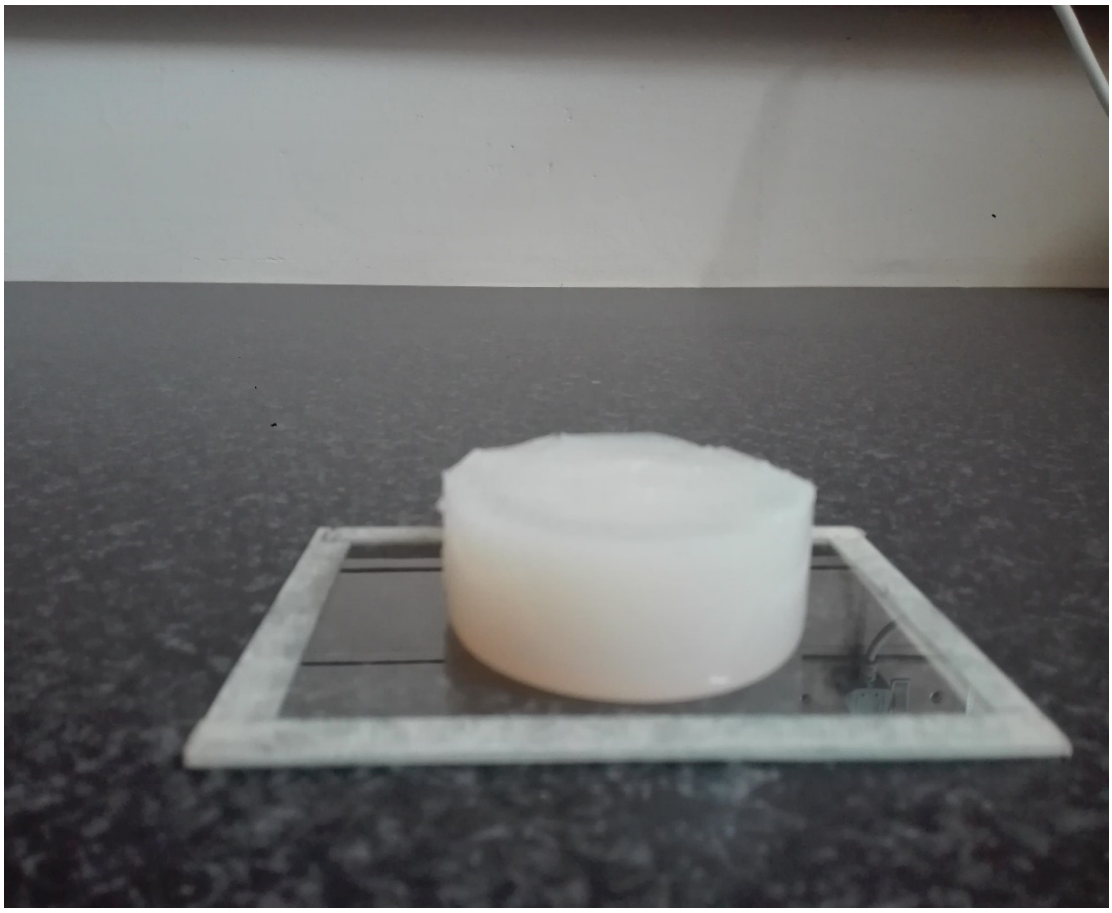

Figure 3. 1: A pure phantom sample

3.2.2 Optical Properties Measurements

The experimental set-up used to investigate the optical properties of the phantom tissue sample is presented in Figure 3.2.

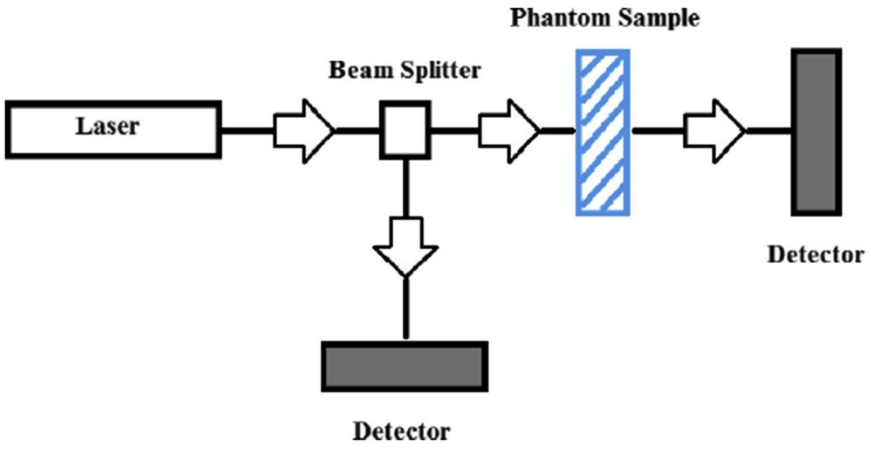

Figure 3. 2: A diagram showing apparatus set up for this experiment [33]

Following fabrication, the samples were sliced into thin slices of different thicknesses with a Stanley knife, and the thickness measured using a digital Vernier caliper. Care was taken during the slicing process to ensure that the tissue integrity is kept intact. The green He-Ne laser light of wavelength 532 nm and the red He-Ne light of wavelength 632 nm were incident on the sliced phantom sample of varying thickness.

The incident beam was divided into two, i.e., by an Edmund Optics (EO 47009), 25-millimeter cube beam splitter, and the intensity of the laser beam incident transmitted through the sample was measured with a digital portable power meter Edmund Optics (EO 54-018).

Comparison between the incident and transmitted power through each slice was sought to understand the attenuation coefficients via the Beer-Lambert law and verify if the sample was an excellent optical simulation of biological tissue [27]:

$$\mu_t = \mu_a + \mu_s , \qquad (3.1).$$

$$= -\frac{1}{L}\ln\left(\frac{P}{P_0}\right)$$

where L is the sample thickness, P_0 is the power of the beam not attenuated, and P is the transmitted light power. For any scattering or absorption (ignoring reflection at the air-tissue surface) events, the intensity or power of light transmitted would be less than the incident

light. The Beer-Lambert law was used in this study, assuming that multiple scattering does not occur and that scattering is instigated by the regular-shaped spherical aluminum oxide (Al_2O_3) particles.

The attenuation was measured for slices of different thicknesses and the average was taken over all slices from a single sample.

For the pure sample, the assumption that

$$\mu_t \approx \mu_s \tag{3.2}$$

was made, considering agar, the base material has mainly intrinsic scattering properties and, thus, its absorption coefficient is much smaller than its scattering coefficient.

Separate samples with Al_2O_3 (scatterers) or black India ink (absorbers) followed by a sample with both were created to investigate the Scattering and Absorbing coefficients and measure the total attenuation coefficient. Measurements of the attenuation coefficients also allowed for the determination of the penetration depth δ [42].

Chapter 4

4. Results

4.1 Measurements

The samples of the optical phantom were created to mimic the optical properties of the brain and prostate tissues. In measuring the optical properties of these simulated samples, a green laser of 532 nm wavelength and a red laser of 630 nm wavelength were used.

Graphs of $-\ln\left(\frac{P}{P_0}\right)$ versus tissue Thickness L were used to investigate attenuation coefficients (μ_t), denoted by the gradient from the best fit line of the graph, with the presumption that summation of absorbing and scattering coefficient contributes in creation of total attenuation coefficient.

4.1.1 Brain Soya Samples

The phantom tissue was firstly made to simulate the optical properties of the human brain at 532 nm. Information of the optical properties may permit for the creation of a brain mimicking model for usage in diagnostic application [32]. The results of these are reflected in Table 4.1.1.

Table 4.1.1: Measurements of the incident and transmitted power through an agar sample made with 100 ml of deionized water and 5.5 g of soy agar using the light of wavelength 532 nm, to investigate the transport coefficient of ink in agar at this wavelength.

Sample Thickness L (mm)	Incident Power P_0 (mW)	Transmitted Power $P(L)$ (mW)	$-\ln\left(\frac{P}{P_0}\right)$	Transport Coefficient $\mu_t\ (\mathrm{cm}^{-1})$
2.98	44.50	14.13	1.147	3.85
5.34	44.34	9.031	1.591	2.98
7.28	44.37	8.024	1.710	2.35
10.48	44.28	4.704	2.242	2.14
15.20	44.30	3.215	2.623	1.73
				Avg = 2.61

The bacteriological agar base material absorption was minimal. Thus, the following presumption $\mu_t \approx \mu_s$ was made.

An explanatory calculation of the sum total attenuation coefficient μ_t in Table 4.1.1 is:

$$\mu_t = -\frac{1}{L}\ln\left(\frac{P}{P_0}\right)$$

$$\mu_t = -\frac{1}{2.98}\ln\left(\frac{14.13}{44.50}\right)$$

$$\mu_t = 0.3849\ \mathrm{mm}^{-1} = 3.85\ \mathrm{cm}^{-1}$$

Graph of $-\ln\left(\frac{P}{P_0}\right)$ versus tissue Thickness L

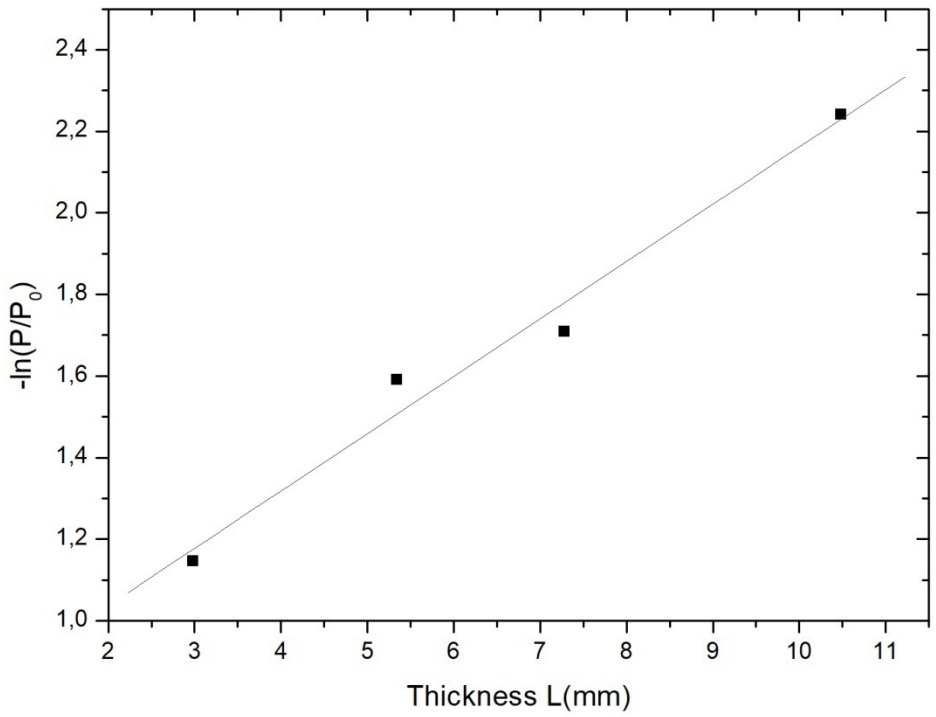

Figure 4.1.1: Graph of $-\ln\left(\frac{P}{P_0}\right)$ versus tissue Thickness for an agar sample made with 100 ml of deionized water and 5.5 g of soy agar

Table 4.1. 2: Measurements of the incident and transmitted power through an agar sample made with 100 ml of deionized water, 5.5 g of soy agar, and 1.8g aluminium oxide using the light of wavelength 532 nm, to investigate the transport coefficient of ink in agar at this wavelength

Sample Thickness L (mm)	Incident Power P_0 (mW)	Transmitted Power $P(L)$ (mW)	$-\ln\left(\frac{P}{P_0}\right)$	Transport Coefficient μ_t $\left(\text{cm}^{-1}\right)$
3.23	44.39	13.10	1.220	3.78
5.21	44.04	8.020	1.703	3.27
7.13	44.57	7.013	1.849	2.59
10.41	44.63	3.602	2.517	2.42
15.13	43.90	2.148	3.017	1.99
				Avg = 2.81

The bacteriological agar base material absorption was minimal and Al_2O_3 negligible. Thus, the following assumption $\mu_t \approx \mu_s$ was made.

Graph of $-\ln\left(\frac{P}{P_0}\right)$ versus tissue Thickness L (Figure 4.1.2) used to measure the attenuation coefficient μ_t, defined by the slope of the linear fit.

Graph of $-\ln\left(\frac{P}{P_0}\right)$ versus tissue Thickness L

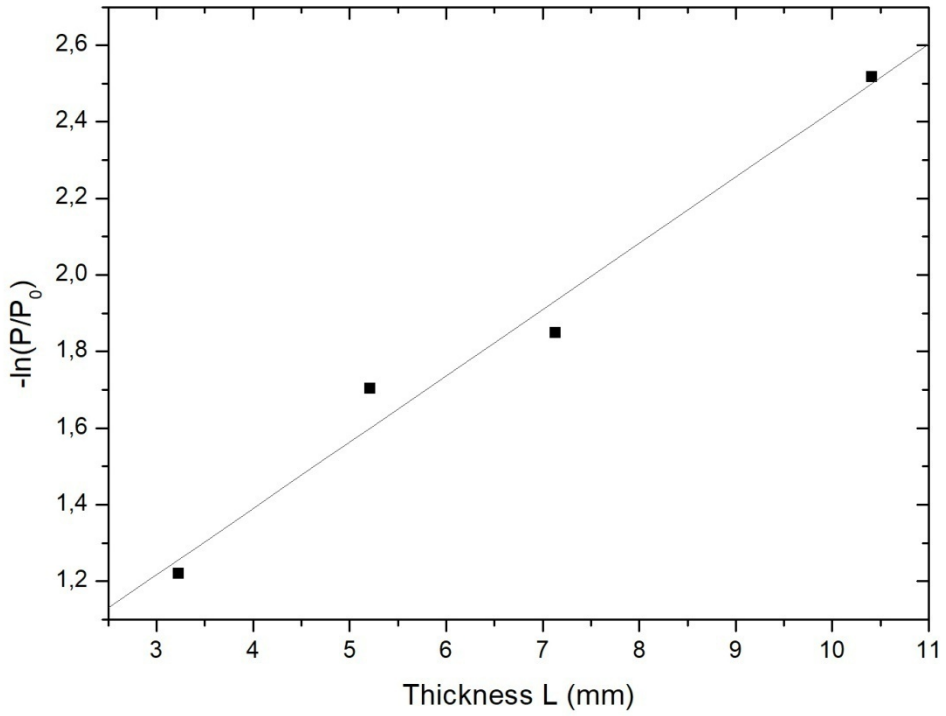

Figure 4.1. 2: Graph of $-\ln\left(\frac{P}{P_0}\right)$ versus tissue Thickness for an agar sample made with 100 ml of deionized water, 5.5 g of soy agar, and 1.8g aluminium oxide

Table 4.1.3: Measurements of the incident and transmitted power through an agar sample made with 100 ml of deionized water, 5.5 g of soy agar, and 3ml ink, using the light of wavelength 532 nm, to investigate the transport coefficient of ink in agar at this wavelength

Sample Thickness L (mm)	Incident Power P_0 (mW)	Transmitted Power $P(L)$ (mW)	$-\ln\left(\frac{P}{P_0}\right)$	Transport Coefficient μ_t (cm^{-1})
3.02	44.28	12.05	1.301	4.31
5.14	43.89	7.013	1.834	3.57
7.25	44.01	6.132	1.971	2.72
10.52	44.56	2.504	2.879	2.74
15.03	43.07	1.352	3.461	2.30
				Avg = 3.13

Graph of $-\ln\left(\frac{P}{P_0}\right)$ versus tissue Thickness L (Figure 4.1.3) used to measure the attenuation coefficient μ_t, defined by the slope of the linear fit.

Graph of $-\ln\left(\frac{P}{P_0}\right)$ versus tissue Thickness $L(\mathrm{mm})$

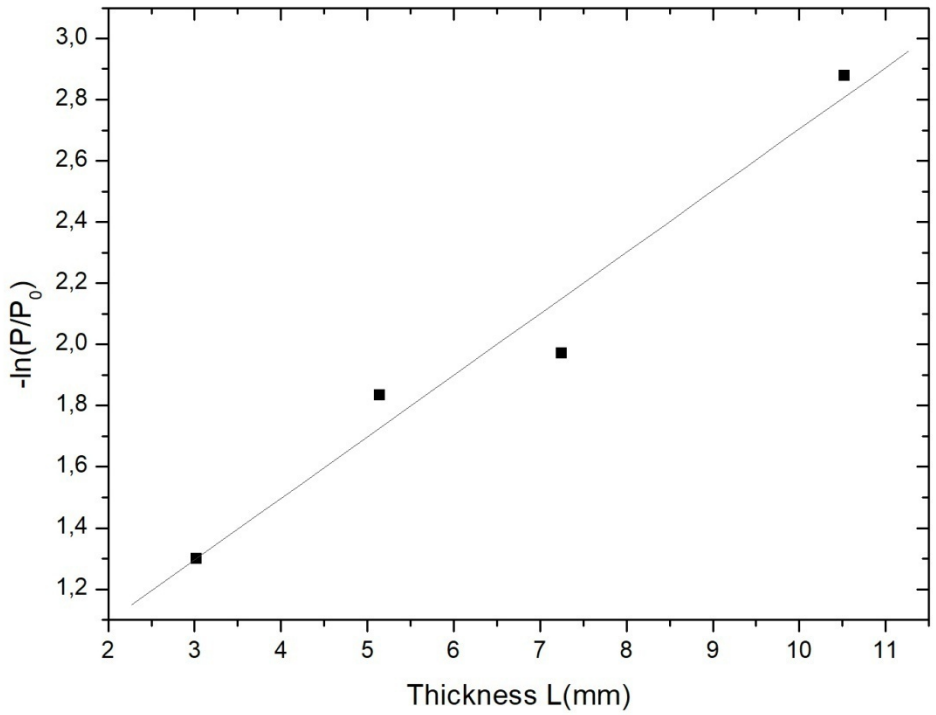

Figure 4.1. 3: Graph of $-\ln\left(\frac{P}{P_0}\right)$ versus tissue Thickness for an agar sample made with 100 ml of deionized water, 5.5 g of soy agar, and 3ml ink

Table 4.1.4: Measurements of the incident and transmitted power through an agar sample made with 100 ml of deionized water, 5.5 g of soy agar, 1.8g aluminium oxide, and 3ml ink,

using the light of wavelength 532 nm, to investigate the transport coefficient of ink in agar at this wavelength

Sample Thickness L (mm)	Incident Power P_0 (mW)	Transmitted Power $P(L)$ (mW)	$-\ln\left(\frac{P}{P_0}\right)$	Transport Coefficient μ_t (cm^{-1})
3.13	44.37	11.07	1.388	4.43
5.51	44.27	6.017	1.996	3.92
7.42	46.47	4.541	2.326	2.91
10.61	44.57	1.767	3.228	3.16
15.07	42.97	0.707	4.107	2.73
				Avg = 3.43

Graph of $-\ln\left(\frac{P}{P_0}\right)$ versus tissue Thickness L (Figure 4.1.2) used to measure the attenuation coefficient μ_t, defined by the slope of the linear fit.

Graph of $-\ln\left(\frac{P}{P_0}\right)$ versus tissue Thickness

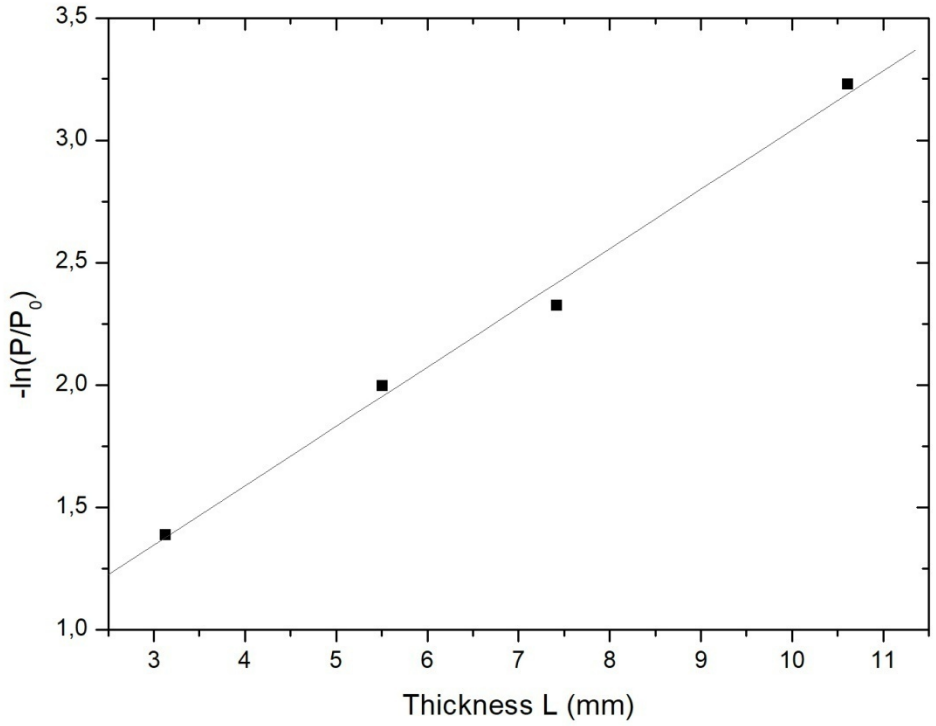

Figure 4.1.4: Graph of $-\ln\left(\frac{P}{P_0}\right)$ versus tissue Thickness for an agar sample made with 100 ml of deionized water, 5.5 g of soy agar, 1.8g aluminium oxide, and 3ml ink

4.1.2 Analysis for Brain Soy agar Samples

4.1.2.1 Attenuation Coefficients

Table 4.1.5: **The attenuation coefficients achieved by calculation as well as graphically from the fit line slope**

Agar Sample	[Calculated] $\mu_t\ (\mathrm{cm}^{-1})$	[Graphical] $\mu_t\ (\mathrm{cm}^{-1})$
Pure	2.61	1.40 ± 0.15
1.8 g of Al_2O_3	2.81	1.73 ± 0.19
3 ml of ink	3.13	2.01 ± 0.28
1.8 g of Al_2O_3 and 3 ml of ink	3.43	2.42 ± 0.14

The phantom tissue with Al_2O_3 and ink has the highest transport coefficient, signifying that the aluminium oxide and ink utilized were effective as scatters and absorbers, respectively.

4.1.3 Penetration Depth

The attenuation coefficient's reciprocal attained in Table 4.1.5 approximates penetration depth, which was then utilised to regulate light transmittance via a tissue.

Table 4.1. 6: Below is the table for the penetration depth of the brain samples, which simply signifies how deep laser light can penetrate the samples

Agar Sample	δ [Calculated]	δ [Graphical]
Pure	0.38	0.71
1.8 g of Al_2O_3	0.36	0.58
3 ml of ink	0.32	0.50

1.8 g of Al_2O_3 and 3 ml of ink	0.30	0.41

The phantom tissue with Al_2O_3 and ink has the lowest penetration depth due to its higher attenuation. The discrepancies between calculated and graphical values are caused by not being able to get the best fit line, so that appropriate transport coefficients can be found. This might be caused by data points being a little bit scattered apart. This means that the precision and accuracy of the results can be bettered by the usage of more sensitive intensity or power meter to permit more significant figures in the measurement of scattering and absorption coefficients.

4.1.4 Absorption Coefficient's Determination

The bacteriological phantom with an India ink (absorber) and Al_2O_3 (scatterer) displayed the highest attenuation in this work, which was in part influenced by bacteriological agar intrinsic scattering properties. The complete phantom sample with India ink and Al_2O_3 had an attenuation coefficient of $\mu_t = 2.40cm^{-1}$ and a scattering coefficient of $\mu_s = 1.73cm^{-1}$, from which it was then possible to determine the absorption attributable to added India ink in the complete phantom.

Applying equation (2.24):

$\mu_a = \mu_t - \mu_s$

= 2.42 – 1.73

= 0.69 cm^{-1}

4.1.5 Optical Albedo

a = μ_s / μ_t

= 1.73/2.42

= 0.71 cm^{-1}

Thus, 71 % of the attenuation in this phantom sample was due to scatterers and the other portion (29 %) was the result of absorption. Addition of more scatterers is not the solution to better the results, because it will lead to dense packing of the scattering centres in the phantom tissues.

4.2 Prostate soya samples

The samples of the optical phantom were created to mimic the optical properties of the prostate tissue. In measuring the optical properties of these simulated samples, a red laser of 630nm wavelength was used.

Graphs of $-\ln\left(\frac{P}{P_0}\right)$ versus tissue Thickness L were used to investigate attenuation coefficients (μ_t), denoted by the gradient from the best fit line from the graph, with the

Sample Thickness L (mm)	Incident Power P_0 (mW)	Transmitted Power $P(L)$ (mW)	$-\ln\left(\frac{P}{P_0}\right)$	Transport Coefficient μ_t (cm^{-1})
3.32	5.336	0.567	2.242	6.75
5.42	5.667	0.486	2.456	4.53
7.36	5.754	0.087	4.192	5.70
10.52	5.745	0.025	5.437	5.17
12.22	5.867	0.005	7.068	5.78
				Avg = 5.59

presumption that summation of absorbing and scattering coefficient contribute in creation of total attenuation coefficient.

Table 4.2.1: Measurements of the incident and transmitted power through an agar sample made with 100 ml of deionized water, 5.5 g of soy agar, using the light of wavelength 630 nm, to investigate the transport coefficient of ink in agar at this wavelength

Graph of $-\ln\left(\frac{P}{P_0}\right)$ versus tissue Thickness L (Figure 4.2.1) used to measure the attenuation coefficient μ_t, defined by the slope of the linear fit.

Graph of $-\ln\left(\frac{P}{P_0}\right)$ versus tissue Thickness L

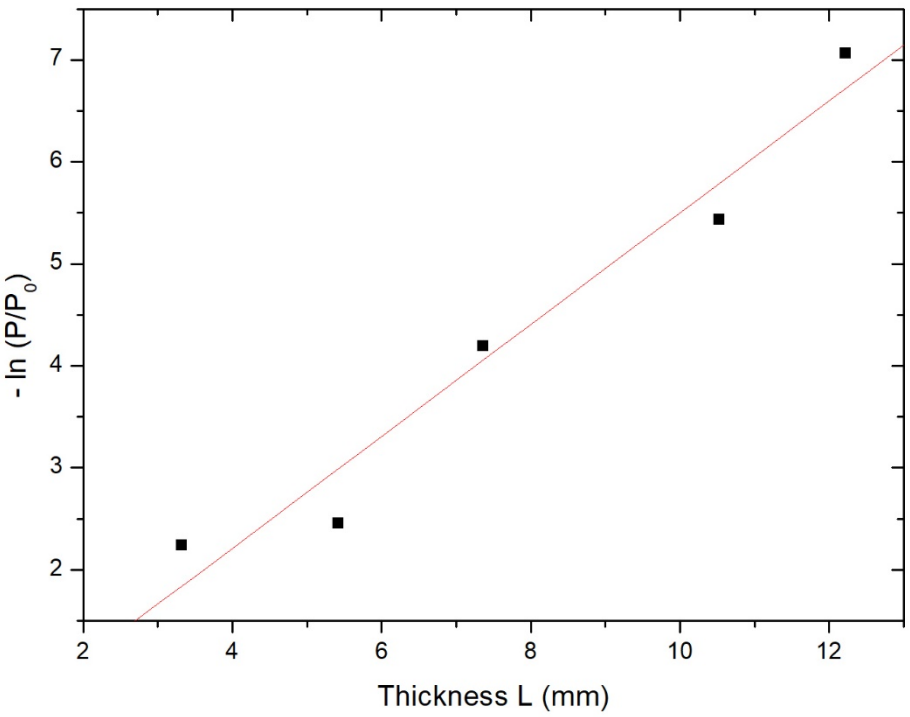

Figure 4.2.1: Graph of $-\ln\left(\frac{P}{P_0}\right)$ versus tissue Thickness for an agar sample made with 100 ml of deionized water, 5.5 g of soy agar

Sample Thickness L (mm)	Incident Power P_0 (mW)	Transmitted Power $P(L)$ (mW)	$-\ln\left(\frac{P}{P_0}\right)$	Transport Coefficient μ_t (cm^{-1})
3.44	5.246	0.457	2.441	7.10
5.53	5.567	0.355	2.752	4.98
7.47	5.817	0.077	4.325	5.79
10.60	5.716	0.014	6.012	5.67
12.43	5.797	0.004	7.279	5.86
				Avg = 5.88

Table 4.2.2: Measurements of the incident and transmitted power through an agar sample made with 100 ml of deionized water, 5.5 g of soy agar, and 2.2g aluminium oxide using the light of wavelength 630 nm, to investigate the transport coefficient of ink in agar at this wavelength

Graph of $-\ln\left(\frac{P}{P_0}\right)$ versus tissue Thickness L (Figure 4.2.2) used to measure the attenuation coefficient μ_t, defined by the slope of the linear fit.

Graph of $-\ln\left(\frac{P}{P_0}\right)$ versus tissue Thickness

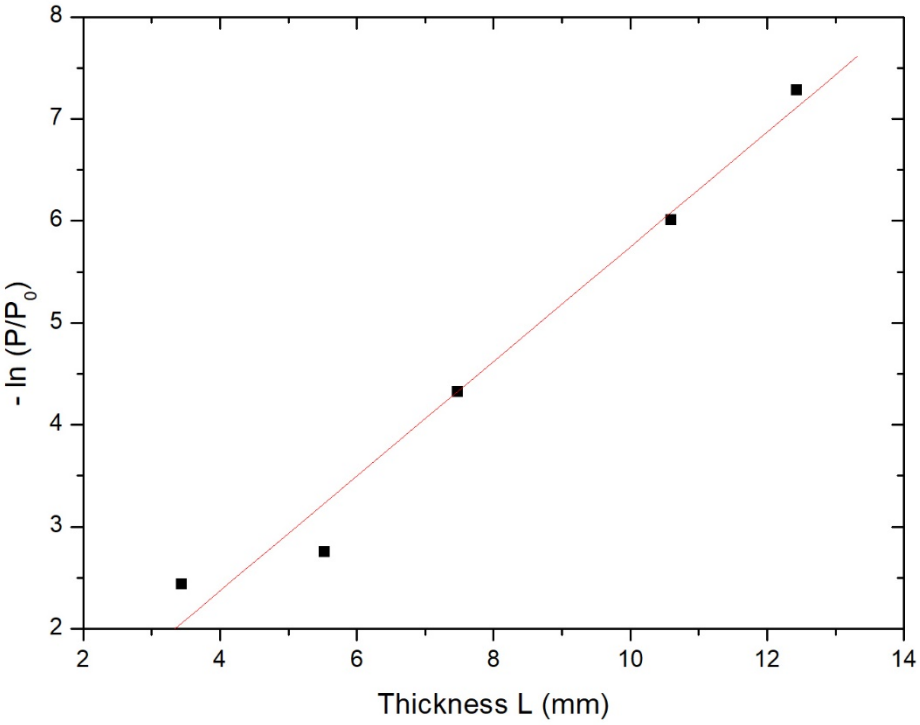

Figure 4.2.2: Graph of $-\ln\left(\frac{P}{P_0}\right)$ versus tissue Thickness for an agar sample made with 100 ml of deionized water, 5.5 g of soy agar, and 2.2g aluminium oxide

Table 4.2.3: Measurements of the incident and transmitted power through an agar sample made with 100 ml of deionized water, 5.5 g of soy agar, and 3ml ink, using the light of wavelength 630 nm, to investigate the transport coefficient of ink in agar at this wavelength

Sample Thickness L (mm)	Incident Power P_0 (mW)	Transmitted Power $P(L)$ (mW)	$-\ln\left(\frac{P}{P_0}\right)$	Transport Coefficient μ_t (cm^{-1})
3.13	5.037	0.367	2.619	8.37
5.45	5.487	0.246	3.105	5.70
7.25	5.607	0.058	4.571	6.30
10.36	5.507	0.008	6.534	6.31
12.30	5.587	0.003	7.530	6.12
				Avg = 6.56

Graph of $-\ln\left(\frac{P}{P_0}\right)$ versus tissue Thickness L (Figure 4.2.3) used to measure the attenuation coefficient μ_t, defined by the slope of the linear fit.

Graph of $-\ln\left(\frac{P}{P_0}\right)$ versus tissue Thickness

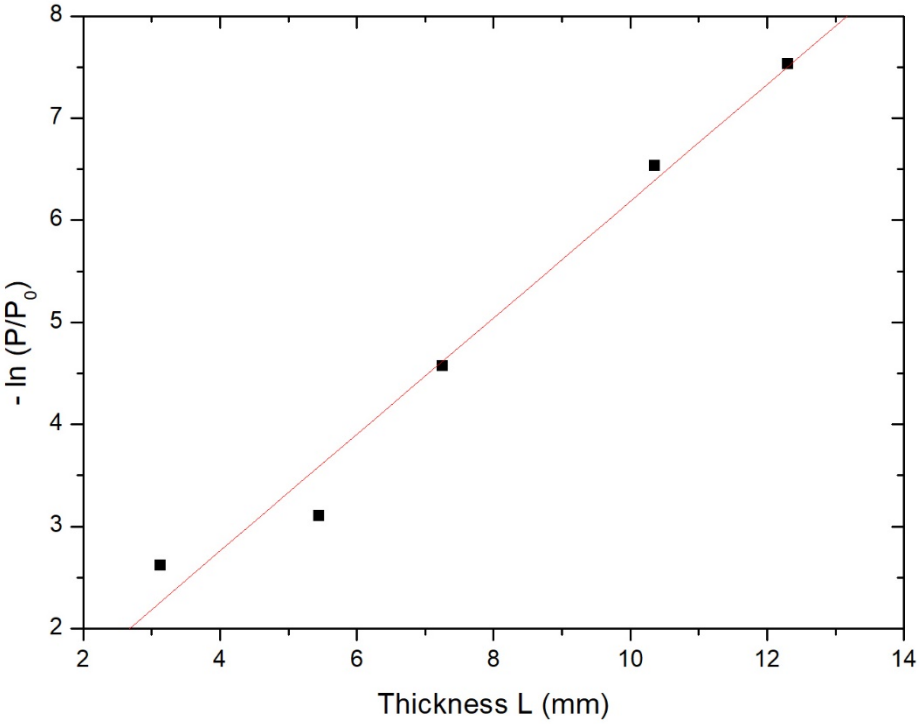

Figure 4.2.3: Graph of $-\ln\left(\frac{P}{P_0}\right)$ versus tissue Thickness for an agar sample made with 100 ml of deionized water, 5.5 g of soy agar, and 3ml ink

Table 4.2. 4: Measurements of the incident and transmitted power through an agar sample made with 100 ml of deionized water, 5.5 g of soy agar, 2.2g aluminium oxide, and 3ml ink, using the light of wavelength 630 nm, to investigate the transport coefficient of ink in agar at this wavelength

Sample Thickness L (mm)	Incident Power P_0 (mW)	Transmitted Power $P(L)$ (mW)	$-\ln\left(\frac{P}{P_0}\right)$	Transport Coefficient μ_t (cm^{-1})
3.33	5.127	0.277	2.918	8.76
5.23	5.397	0.127	3.749	7.17
7.05	5.507	0.047	4.764	6.76
10.41	5.607	0.007	6.686	6.42
12.09	5.567	0.002	7.931	5.26
				Avg = 6.87

Graph of $-\ln\left(\frac{P}{P_0}\right)$ versus tissue Thickness L (Figure 4.2.4) used to measure the attenuation coefficient μ_t, defined by the slope of the linear fit.

Graph of $-\ln\left(\frac{P}{P_0}\right)$ versus tissue Thickness

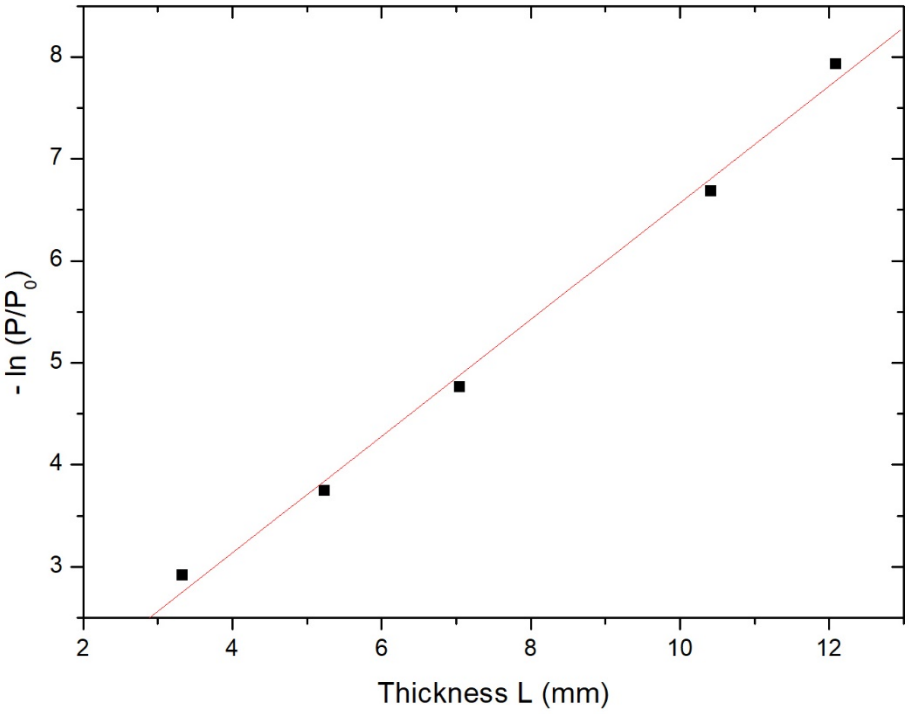

Figure 4.2.4: Graph of $-\ln\left(\frac{P}{P_0}\right)$ versus tissue Thickness for an agar sample made with 100 ml of deionized water, 5.5 g of soy agar, 2.2g aluminium oxide, and 3ml ink

4.2.1 Analysis for Prostate Soy Agar Samples

Table 4.2.5: Table of calculated and graphical values for prostate soy agar samples

Agar Sample	[Calculated] $\mu_t\ (\mathrm{cm}^{-1})$	[Graphical] $\mu_t\ (\mathrm{cm}^{-1})$
Pure	5.59	5.48 ± 0.67
2.2 g of Al_2O_3	5.88	5.62 ± 0.51
3 ml of ink	6.56	5.71 ± 0.48
2.2 g of Al_2O_3 and 3 ml of ink	6.87	5.72 ± 0.24

The phantom tissue with Al_2O_3 and ink has the highest transport coefficient signifying that the aluminium oxide and ink utilized were effective scatter and absorber, respectively.

4.2.2 Penetration Depth

The attenuation coefficient's reciprocal attained in Table 4.2.6 approximates penetration depth, which was then utilised to regulate light transmittance via a tissue.

Table 4.2.6: Below is the table for the penetration depth of the brain samples, which simply signifies how deep laser light can penetrate the samples.

Agar Sample	δ [Calculated]	δ [Graphical]

Pure	0.18	0.182
5.5 g of Al_2O_3	0.17	0.178
3 ml of ink	0.15	0.175
5.5 g of Al_2O_3 and 3 ml of ink	0.15	0.175

The phantom tissue with Al_2O_3 and ink has the lowest penetration depth because of its higher attenuation.

4.2.3 Absorption Coefficient's Determination

The agar also contributes to the scattering of a phantom tissue. Pure agar has the lowest scattering attenuation (μ_s = 5.48). The complete phantom sample with India ink and Al_2O_3 had an attenuation coefficient of $\mu_t = 5.72\ \mathrm{cm}^{-1}$ and a scattering coefficient of $\mu_s = 5.48\ \mathrm{cm}^{-1}$, from which it was then possible to determine the absorption attributable to added India ink in the complete phantom.

Applying equation (2.24):

$\mu_a = \mu_t - \mu_s$

= 5.72 - 5.48

= 0.24 cm^{-1}

4.2.4 Optical Albedo

a = μ_s / μ_t

= 5.48/5.72

= 0.96

Thus, 96 % of the attenuation in this phantom sample was because of scatterers and the other portion (4 %) was the result of absorption.

Chapter 5

5.1 Discussion

Table 5.1 shows the penetration depths of brain tissues from previous theories to compare them with the current study.

Table 5.1: Consideration of similarities of penetration depth δ with other authors' values for the brain.

Wavelength (nm)	Penetration depth δ	References
514	0.4 - 0.6	[33]
980	14	[42]
810	38.1	
660	32.8	
835	2.52 ± 0.19	[43]
780	2.17 ± 0.16	
675		
632.8	1.38 ± 0.13	
	0.92 ± 0.08	
808		[44]
	40	

The attenuation coefficient values established (in Table 4.1.1) ranged between 1.73 and 3.85 cm^{-1} which is reasonably within the range by Becky T et al. (Table 5.2) [49]. The penetration depth for the brain phantom tissue of the calculated values in Table 4.1.6 (0.30 - 0.38) at 532 nm is approximately within the range (0.4 – 0.6) brain tissue at 514 nm wavelength, in Table 5.1 [33]. This comparison was made because the two wavelengths (532nm and 514 nm) are not too far apart in magnitude. The recorded data points were connected by a straight line to investigate the attenuation coefficients μ_t described as the gradient of the linear curve. The penetration depth of the 532nm laser light in the fabricated brain tissue with scattering and

absorption coefficients (μ_s and μ_a) of 1.73 cm^{-1} and 0.69 cm^{-1} [45] was found to be approximately 0.4 mm. This indicates that tissue structures situated at a depth larger than approximately 0.4 mm will possibly not have significant photons detected. A comparison between penetration depths in the brain's tissue detailed from this study and literature at various wavelengths is outlined in Table 5.1.

The penetration depth for the brain simulating tissue is lower than those mentioned in the human cadaver brain by Tedford et al. [44]. This might be due to sampling thickness, structures, various manipulations, and the emission source included as the penetration of light in a targeted tissue is a function of the parameters mentioned [43, 46, and 47]. The penetration depth of the calculated values in Table 4.1.6 (0.30 - 0.38) is approximately within the range like the ones at 512 nm wavelength, in table 5.1 (0.4 – 0.6) [33]. The attenuation coefficients (ranges between 5.48 and 5.72 cm^{-1}) found in Table 4.2.5 are relatively comparable to those in Table 5.2 by Lee et al. [50]. The scattering and absorption coefficients (μ_s and μ_a) for complete phantom tissue (presented in Table 4.2.5) show that the tissue was fabricated to mimic the prostate tissue of the human being. Here μ_s = 5.48 cm^{-1} and μ_a = 0.24 cm^{-1}, which respectively fall within the accepted values of scattering and absorption for the prostate tissue [50].

5.1 Error Analysis

In this project, some few challenges were encountered while setting up the experiment. However, adequate efforts were made to lessen the source of errors that were likely to emerge.

Error Origin

Some errors encountered in this work comprise extra particles coming from deionized water for preparation of phantom, the uneven of slice thicknesses, and the unsteady stabilization of the laser check employed for the power intensity measurement. Fluctuation of the laser beam due to wind turbulence and heating as well as the irregular distribution of the quantity of scatter and absorber that were added to the samples of the phantom may have contributed to errors encountered. Table 5.2 shows scattering and absorption coefficients of different phantom tissues at close wavelengths for previous studies to the ones used in this study. This is for comparison with absorption and scattering coefficients calculated from this study.

Table 5.2: Optical properties of human being tissue from different sources

$\lambda(\mathrm{nm})$	$\mu_a(\mathrm{cm}^{-1})$	$\mu_s(\mathrm{cm}^{-1})$	Tissue	Source
532	0.02 - 3.84	0.10 – 46.3	brain	Becky T et al. [49]
420	0.01 – 3.51	18.75 – 55.83		
630	0.02 - 0.50	3.72 - 21.97		Sandel et al. [46]
760	0.11 – 0.17	4.0 – 10.5		
780	0.078 – 0.089	8.42 – 9.16		
630	0.05-1.0	3.41-17.02	prostate	Sandel et al. [46]
650	0.14 – 0.61	5.24 – 22.68		
672	0.09 – 0.72	7.1 – 25.0		
732	0.09 – 0.72	3.37 – 29.8		
762	0.11 – 1.6	1.2 – 40.0		
630	1.5	386	White matter	Yaroslavsky at al. [50]

665	1.3	1246	blood	Reynolds et al. [51]
514	1.3	190	Bone (skull)	Roggan et al. [52]
633	1.4	88	bladder	Cheong et al. [53]
510	1.0	426	White matter (post mortem)	Yaroslavsky et al. [50]
510-610	0.6-0.9	176.3-188.7	thalamus	Gebhart et al. [54]
500-600	0.6-0.9	109.4-133.7	pons	Gebhart et al. [54]
550	0.67	11.4	Lyposyn plus blood	Kienle et al. [55]
500	1.06	15.35	hypodermis	Paquit et al. [56]
520	0.6	6.51	Epidermis (caucasian skin)	Salomatina et al. [57]
550	1.1	18.48	Dura mater (adult head)	Bashkatov and Genina et al. [58]
530	1.14	18.4	Healthy tissue adjacent to invasive ductal carcinoma	Das, Liu and Alfano [59]

Absorption and scattering coefficient values and other optical properties might be distinctive to definite tissues or tumors. Therefore, a realization of the optical properties of an assembly of cancer cells can permit added research to disclose the likelihood of treatment and tum diagnosis. Absorption is easily varied through different amounts of black India ink. Scattering coefficients are much more significant than those in this project.

Increasing the amount of Al_2O_3 also increases the scattering of the phantom. Likewise, when the India black ink has increased, the absorption of the sample also increased. The result's accuracy and precision might be enhanced using an added sensitive power meter to permit other important figures in the absorption calculation and scattering coefficients. The laser power oscillates by Mw, all through a solitary experimental method.

More measurements should also be performed to improve the average transport coefficient. The results can be further enhanced with a cost-effective automatic stirrer or better cutting techniques/devices.

Chapter 6

6.1 Conclusion

Generally, tissue-mimicking samples are easy to create and give expected results with visible lights. The optical attributes of the tissues might be simulated with appropriate absorption and scattering coefficients. This work investigated the biochemical mechanisms of light tissue interactions by fabricating phantoms with optical properties comparable to the human brain and prostate tissues. Obtaining an accurate distribution of light in tissues presents a considerable problem for optical spectrum in diagnostics and therapeutic applications. The phantoms recipes and set-up for optical characteristics through cost-effective materials and apparatus produce valuable and repeatable data. The considerable differences observed in the phantoms' optical behavior show the need to have accurate information to optimize laser therapy and phototherapy in general, depending on the wavelength and tissue type. Moreover, an integrating sphere might be incorporated into the experimental arrangement to obtain the anisotropy factor g and the reduced absorption and scattering coefficients.

References

1. Laal M Innovation process in medical imaging. *Procedia-Social and Behavioural Sciences,* 81:pp.60–64, 2013.

2. Welch AJ, Torres JH, Cheong W. Laser Physics and Laser-Tissue Interaction. Texas Heart Institute Journal. 1989; 16:141-9.
3. Hutchison AM, Beard DJ, Bishop J, Pallister I, Davies W. An Investigation of the Transmission and Attenuation of Intense Pulsed Light on Samples of Human Achilles Tendon and Surrounding Tissue. Lasers in Surgery and Medicine. 2012; 44.
4. Kim A, Keller JB. Light Propagation in Biological Tissue. Departments of Mathematics and Mechanical Engineering Stanford University, USA.
5. Ghosh S, Soni J, Purwar H, et al. Differing Self-similarity in Light Scattering spectra: A Potential.
6. Chen Chen, Florian Klampfl, Christian Knipfer, Max Riemann, Rajesh Kanawade, Florian Stelzle, and Michael Schmidt. Preparation of a skin equivalent phantom with interior micro-scale vessel structures for optical imaging experiments.
7. El-Bendary M. A.M.Kasban, H.and D.H.Salama. A comparative study of medical imaging techniques. Int. J. Inf. Sci. Intell. Syst., 4(2):pp.37–58, 2015.
8. Pogue BW, Patterson MS. Review of tissue simulating phantoms for optical spectroscopy, imaging and dosimetry. J Biomed Opt 2006; 11(4):041102.
9. Cubeddu, R., Pifferi, A., Taroni, P., Torricelli, A., and Valentini, G., "A solid tissue phantom for photon migration studies," Physics in Medicine and Biology 42(10), 1971 (1997).
10. Niemz MH. Laser-Tissue Interactions: Fundamentals and Applications. 3rd ed. Springer. 2007.
11. Wilson BC, Tuchin VV, Tanev S. Advances in Biophotonics. (Eds.) IOS Press. 2005.
12. Pravdin AB, Chernova SP, Papazoglou TG, Tuchin VV. Handbook of Optical Biomedical Diagnostics. Chapter 5: Tissue Phantoms. Bellingham: SPIE; 2002.
13. Jephias Gwamuri, Prof. Ashok V Gholap, Dr Tahami S Mohamed Shartir, and Prof Paul K Bauh-Bassuah. Investigating light propagation in turbid media by evaluation optical properties of phantom tissues. 2014.
14. Tuchin VV. Tissue Optics: Light Scattering Methods and Instruments for Medical Diagnosis. 2nd ed. Bellingham: SPIE; 2007.
15. Taylor EF. Illumination Fundamentals. Rensselaer Polytechnic Institute. 2000.

16. Spectrophotometry. [Found on the internet]. Available from http://chemwiki.ucdavis.edu/Physical_Chemistry/Kinetics/Reaction_Rates/Experimental_Determination_of_Kinetcs/Spectrophotometry.
17. Kim A, Keller JB. Light Propagation in Biological Tissue. Departments of Mathematics and Mechanical Engineering Stanford University, USA.
18. Sviridov A, Hassan VCM, Russo A, et al. Intensity Proles of Linearly Polarized Light Backscattered from Skin and Tissue-like Phantoms. Journal of Biomedical Optics. 2005; 10(1).
19. Bass M. Handbook of Optics Volume II: Devices, Measurements, and Properties 2nd ed. United States of America: McGraw-Hill, inc. 1995.
20. Wilson BC, Patterson MS. The physics of photodynamic therapy. Phys Med Biol 1986; 26:327–60.
21. Tromberg BJ, Svaasand LO, Fehr MK, Madsen SJ, Wyss P, Sasone B, Tadir YA. Mathematic model for light dosimetery in photodynamic destruction of human endometrium. Phys Med Biol 1996;41:233–7.
22. Baranoski GVG, Krishnaswamy A. An introduction to light Interaction with Human skin. RITA. 2004.
23. Biomedical Engineering, The University of Arizona. [Found on the internet]. Available from https://wp.optics.arizona.edu/winter-school-workshop/wp-content/uploads/sites/16/2015/09/Biomedical-Optics-winter-school-2015-smaller-1.pdf
24. Bass M. Handbook of Optics Volume I: Fundamentals, Techniques, and Design 2nd ed. United States of America: McGraw-Hill, inc. 1995.
25. UCL Department of Medical Physics and Bioengineering. [Found on the internet]. Available from http://www.medphys.ucl.ac.uk/research/borl/homepages/florian/thesis/pdf_files/p45_58.pdf.
26. Mitic G, Wolfgang J, Kolzer Z, Otto J, Plies E, Solkner G. Time-gated Transillumination of Biological Tissues and Tissue like Phantoms. Applied Optics. 1994; 38.
27. Koval G, Blair G, Jacques SL, et al. In Vivo Determination of Optical Properties of Normal and Tumor Tissue with White Light Re ectance and an Empirical Light Transport Model during Endoscopy. Journal of Biomedical Optics. 2005; 10(3).

28. Jacques SL. Optical Properties of Biological Tissues: A Review. Physics in Medicine and Biology. 2013; 58.
29. Tuchin VV, Zimnyakov DA, Wang LV. Optical Polarization in Biomedical Applications. Springer. 3rd ed. 2006.
30. Frederick Ayers, Alex Grant, Danny Kuo, David J. Cuccia, Anthony J. Durkin Laser Microbean, Medical Program, Beckman Laser Institute, UniversityofCA,IrvineModulatedImaging,Inc.,AlisoViejo,CA,andBeckmanLaser Institute Photonic Incubator. Fabrication and characterization of silicone-based tissuephantomswithtunableopticalpropertiesinthevisibleandnearinfrared domain. International Society for Optics and Photonics. 6870:687007, 2008.
31. Hartleb C. Creation and Evaluation of Solid Optical Tissue Phantoms for Bio-medical Optics Applications. Ilmenau University of Technology. 2005.
32. L.O.Svaasand and R.Ellingsen. Optical properties of human brain. *Photochem*. *Photobiol*, 38(3):pp.293–299, 1983.
33. P.Wang Y.LiT.Li, C.Xue and L.Wu. Photon penetration depth in human brain for light stimulation and treatment: A realistic Monte Carlo simulation study. J. Innov. Opt. Health Sci, 10(5), 2017.
34. College of Life Science, National Tsing Hua University. [Found on the internet]. Available from http://life.nthu.edu.tw/~labcjw/BioPhyChem/Spectroscopy/beerslaw.htm.
35. American Cancer Society [found on the internet] Available from http://www.cancer.org/treatment/treatmentsandisideeffects/treatmentypes/lasers-in-cancers-treatment.
36. James NS, Ohulchanskyy TY, Chen Y, et al. Comparative Tumor Imaging and PDT E-cacy of HPPH Conjugated in the Mono- and Di-Forms to Various Polymethine Cyanine Dyes: Part - 2. Theranostics 2013; 3(9):703-718. [Found on the internet]. Available from http://www.thno.org/v03p0703.htm.
37. Avanaki MRN, Hojjat A, Podeleanu AG. Multilayer Tissue-Like Optical Phantom; a Model for Skin in Optical Coherence Tomography Imaging. Microscopy Focus. 2010.

38. Ayers F, Grant A, Kuo D, Cuccia DJ, Durkin AJ. Fabrication and Characterization of Silicone-based Tissue Phantoms with Tunable Optical Properties in the Visible and Near Infrared Domain. SPIE; 6870 6870072.
39. Ramakrishna SA, Rao KD. Pramana Journal of Physics. Estimation of Light Transport Parameters in Biological Media using Coherent Backscattering. 2000; 54.
40. Alireza Mowla, Thomas Taimre, Yah Leng Lim, Karl Bertling, Stephen J. Wilson, Tarl W. Prow, H. Peter Soyer, and Aleksandar D. Rakić "Diffuse reflectance imaging for non-melanoma skin cancer detection using laser feedback interferometry", Proc. SPIE 9887, Biophotonics: Photonic Solutions for Better Health Care V, 98870T (27 April 2016); https://doi.org/10.1117/12.2227449.
41. Kodach, V. M. (2012). Development of functional near-infrared optical coherence tomography.
42. A. Perez S.Stolik, J.A. Delgado and L.Anasagasti. Measurement of the penetration depth so fred and near-infrared light in human ex vivo tissues. J.Photochem. Photobiol. B: Biology, 57:9093, 2000.
43. S.Jacques C.E.Tedford, S.DeLappand J.Anders. Quantitative analysis of transcranial and intraparenchymal light penetration in human cadaver brain tissue. Lasers Surg. Med, 47(4):pp. 312–322, 2015.
44. T.C. Zhu Sandell. A review of in-vivo optical properties of human tissues and its impact on pdt. 4:773787, 2011.
45. J. Wagner H. Kolrov, D. Ditrichov. Penetration of laser light into the skin in vitro. Lasers Surg Med, 8(7):24:231235, 1999.
46. J.M. Wininger D.E. Hudson, D.O. Hudson and B.D. Richardson. Penetration of laser light at 808 and 980 nm in bovine tissue samples. Photomed Laser Surg, 31(4):1638, 2013.
47. L.O.Svaasand and R.Ellingsen. Optical properties of human brain. Photochem. Photobiol, 38(3):pp.293–299, 1983.
48. Reynolds LO, Johnson CC, Ishimaru A. Diuse Reectance from a Finite Blood Medium: Applications to the Modeling of Fiber Optic Catheters. Applied Optics. 1976.
49. J.L. Sandell and T.C. Zhu. A review of in-vivo optical properties of human tissues and its impact on pdt. J Biophotonics, 4(1112):773787, 2011.

50. Bashkatov AN. Controlling of Optical Properties of Tissues at Action by Osmotically Active Immersion Liquids. Cand. Science Thesis, Saratov State Univ. Saratov. 2002.
51. Roggan A, Albrecht H, Dorschel K, Minet O, Muller G. Experimental Set-up and Monte-Carlo Model for the Determination of Optical Tissue Properties in the Wavelength Range 3301100 nm. Proc. SPIE 2323. 1995.
52. Cheong WF, Motamedi M, Welch AJ. Optical Modeling of Laser Photocoagulation of Bladder Tissue. Lasers in Surgery and Medicine. 1987.
53. Yaroslavsky AN, Schulze PC, Yaroslavsky IV, Schober R, Ulrich F, Schwarzmaier HJ. Optical Properties of Selected Native and Coagulated Human Brain Tissues In Vitro in the Visible and Near Infrared Spectral Range. Physics in Medicine and. Biology. 2002; 47.
54. Gebhart SC, Lin WC, Mahadevan-Jansen A. In Vitro Determination of Normal and Neoplastic Human Brain Tissue Optical Properties Using Inverse Adding-Doubling. Phys. Med. Biol. 2006; 51.
55. Kienle A, Lilge L, Vitkin I, et al. Why Do Veins Appear Blue? A New Look at Old Question. Appl. Opt. 1996; 35: No. 7.
56. Paquit VC, M´eriaudeau F, Price JR, Tobin KW. Simulation of Skin Reectance Images using 3D Tissue Modeling and Multispectral Monte Carlo Light Propagation. Conf Proc IEEE: Engineering in Medicine and Biology Society. 2008.
57. Salomatina E, Jiang B, Novak J, Yaroslavsky AN. Optical Properties of Normal and Cancerous Human Skin in the Visible and Near Infrared Spectral Range. J. Biomed. Opt. 2006.
58. Genina EA, Bashkatov AN, Kochubey VI, Tuchin VV. Optical Clearing of Human Dura Mater. Opt. Spectrosc. 2005; 98: No. 3.
59. Das BB, Liu F, Alfano RR. Time-Resolved Fluorescence and Photon Migration Studies in Biomedical and Random Media. Rep. Prog. Phys. 1997; 60.
60. A.H. Hielscher, A.Y. Bluestone. Near-infrared diffuse optical tomography. Disease Makers.2002.
61. Transmittance. [Found on the internet] Available from https://www.edinst.com/wp-content/uploads/2019/08/BLL-1.png.